R & M No.3814

R & M No.3814

PROCUREMENT EXECUTIVE, MINISTRY OF DEFENCE

Aeronautical Research Council
Reports and Memoranda

NON-CONICAL FLOW PAST SLENDER WINGS WITH LEADING EDGE VORTEX SHEETS

by

R.W. Clark

Aerodynamics Department, RAE Farnborough, Hants

London: Her Majesty's Stationery Office
1978

PRICE £5 NET

NON-CONICAL FLOW PAST SLENDER WINGS WITH LEADING-EDGE VORTEX SHEETS

By R.W. Clark

Aerodynamics Department, RAE Farnborough, Hants

Reports and Memoranda No.3814*

March 1976

SUMMARY

The vortex-sheet model of leading-edge separation which has been successfully applied to slender delta wings of conical shape is extended to non-conical wings which have thin, uncambered cross-sections. Calculations of the shape and strength of the vortex sheet are presented for examples (a) of a plane wing with a curved leading edge and (b) of a delta wing with lengthwise camber. In each case it is found that the sign of the circulation shed from the leading edge changes as the calculation proceeds downstream, but the consequences are very different in the two cases. An experimental investigation to clarify the behaviour of the cambered wing is described.

* Replaces RAE Technical Report 76037 - ARC 36863

CONTENTS

1 INTRODUCTION

The vortex sheet model of separated flow over slender delta wings developed by Smith[1] has been successfully applied to several conical flow problems. The simpler model of Brown and Michael[2] in which the vorticity is assumed to be concentrated into an isolated vortex above each half of the wing has been extended by Smith[3] to treat plane wings with curved leading edges. This paper presents a similar extension of the vortex-sheet model to non-conical wings, enabling separated flow over thin wings with both curved leading edges and lengthwise camber to be calculated. Apart from the limitations implied by the use of slender-body theory, the only restriction on the wing is that its cross-sections are thin and flat.

As in the conical-flow applications, the assumptions of slender-body theory are retained. The vorticity in the primary vortex shed from the leading edge is assumed to be concentrated into an infinite spiral sheet, with the outer part represented explicitly in the numerical calculation, the infinite inner part of the sheet being replaced by an isolated vortex filament. Secondary separation is not represented. The boundary conditions on the sheet follow from the fact that it is a stream surface and that it can sustain no pressure discontinuity. These conditions have been formulated by Smith[4] for a general vortex sheet under the slender-body assumptions and this derivation is outlined in Appendix A. Concentrating the vorticity from the inner part of the sheet into a single vortex filament leaves behind a cut, across which the velocity potential is discontinuous. When the strength of the vortex filament varies, the pressure is also discontinuous across the cut. The force to which this gives rise is balanced by a force acting on the vortex filament, so that the condition of zero pressure difference across the sheet is replaced, for the inner part, by a condition of zero total force. When suitable initial conditions are prescribed, these conditions, together with a leading-edge Kutta condition, provide a set of equations which determine the streamwise evolution of the vortex sheet.

At any streamwise station the velocity field is determined completely in terms of a set of basic variables which define the position and strength of the vortex sheet and of the isolated vortex. The boundary conditions described above relate the streamwise derivatives of these variables to the variables themselves. However an attempt to integrate the equations directly by an explicit integration formula failed because of instability. The difficulty was overcome by the use of an implicit integration technique in which an iterative

method is used to obtain the solution at one streamwise station before proceeding to the next station. When the streamwise derivatives are approximated by a backward-difference formula the set of boundary conditions can be written as a set of non-linear equations in terms of the basic variables, and these equations are solved using a multi-dimensional extension of Newton's iterative method as used by Pullin[5] and Barsby[6] for their conical flow calculations. The initial conditions for this downstream integration are provided by the conical solutions derived by Smith[1]. A similar approach is used by Jones[7] in his work on rolling wings with leading-edge separation.

The method has been applied to various conical and non-conical configurations and in each case it has been found to produce a smooth development of the vortex sheet with results which are almost identical for different streamwise steplengths. When applied to conical wings it was found that if the initial solution was slightly perturbed the calculation would settle down to the known conical solution as the integration proceeded downstream. The results presented include those for plane wings with curved leading edges and delta wings cambered in the streamwise direction.

Several other approaches have been applied to the representation of non-conical leading-edge separation, and a number of them are summarized below. One alternative representation is that adopted by Sacks *et al.*[8]. Instead of using a continuous vortex sheet, they introduce discrete vortex filaments shed at intervals along the leading edge. The subsequent positions of these filaments are followed downstream, so as to represent the roll-up of the vortex sheet. This method still uses slender-body theory and it has the additional disadvantage that the representation of the flow close to the apex is inadequate because of the overall limitations on the number of vortices that can be handled. This means, for instance, that a conical flow cannot be reproduced exactly by such a method. As the number of vortices in the calculation is increased the solution found no longer represents a coherent vortex sheet. This difficulty is avoided in the method presented here by removing the coupling between the vorticity of the sheet and the points defining the sheet. With a vortex-sheet model the vorticity can be convected around the sheet into the isolated vortex without disturbing the points defining the vortex sheet.

The number of vortices which can be handled without losing the coherence of the sheet, has been increased in the vortex filament representation used by Fink and Soh[9] by means of an interpolation procedure applied after each

downstream step. In the calculation of the induced velocity at a point on the vortex sheet by any numerical method it is necessary to include the effect of the interval around the point. In general, this involves a logarithmic singularity. If the velocity is calculated at the mid-point of the interval then this contribution vanishes. Fink and Soh[9] therefore argue that the point vortex calculation will correspond to the numerical approximation of the sheet calculation if the vortices are equally spaced. After each integration step they therefore redistribute the vorticity by interpolation to obtain an equivalent set of equally-spaced vortices. By this means the stability of the numerical calculation is improved. The representation is still inadequate because of both the small number of vortices used close to the apex and the absence of any distinct representation of the central core, the importance of which was emphasised by Moore[10]. Modifications to cover both of these points could however be incorporated into this kind of vortex-filament model.

These methods all use the assumptions of slender-body theory and so make no allowance for any upstream influence. In particular, the validity of the solutions is reduced by the upstream influence of the trailing edge in subsonic flow. The method used by Rehbach[11] avoids this limitation. He considers an incompressible, three-dimensional flow and represents the leading-edge separation by semi-infinite vortex filaments springing from the leading edge and continuing downstream into the wake. The wing is represented by a vortex lattice. The three-dimensional nature of the flow is taken into account in calculating the influence of each of the vortex filaments. As with the other isolated vortex methods this will not give an adequate representation near the apex, and for a flow which is approximately conical the vortex positions predicted seem to be too far inboard. At the trailing edge, however, the positions of the vortices are close to those observed; and Rehbach[11] is able to predict the overall lift successfully. He does not present values of the circulation or pressure distribution over the wing.

An alternative approach to the fully three-dimensional problem is adopted by Rubbert *et al.*[12]. They represent the wake and the leading-edge shear layer by a doublet sheet, with an isolated vortex to represent the rolled-up core. The position of this isolated vortex is fixed in relation to the end of the sheet and an iterative method is used to find the position and strength of the doublet sheet. Although this approach leaves unbalanced forces in the fluid, the results so far reported are in good agreement with experiment.

The method presented here is claimed to be more accurate than those previous methods for non-conical flow which are also based on the assumptions of slender-body theory. It is liable to error through its use of slender-body theory when significant upstream influence occurs, but it gives a more detailed account of the flow development than existing methods which take account of upstream influences.

2 THE MATHEMATICAL FORMULATION

Under the slender-body assumptions the streamwise derivatives are small compared with those in the transverse directions and the velocity can be represented by a potential which satisfies Laplace's equation in the cross-flow plane perpendicular to the free stream. The flow separation is represented by a rolled-up vortex sheet springing from each leading edge with the infinite inner part of each of these sheets being replaced by an isolated vortex joined to the end of the outer part of its sheet by a cut. This cut, which is required to ensure that the velocity potential is single valued, can be regarded as a surface carrying transverse vorticity, but no axial vorticity.

The non-conical wings considered here affect the flow only through the streamwise variation of the span and position of the local cross-section of the wing. The wing and the axes used are shown in Fig.1, the axes $O'xy'z'$ being centred on the apex and $O'x$ aligned with the free stream. The local axes Oyz are introduced in the cross-flow plane as in Fig.2a and are related to the axes through O' by

$$y = y'$$

$$z = z' + h(x) \qquad (2\text{-}1)$$

where $h(x)$ is the distance of the wing centre line below $O'x$. The local angle of incidence of the wing to the free stream, assumed to be small, is therefore given by $h'(x)$.

2.1 The velocity potential

The velocity potential will satisfy the two-dimensional form of Laplace's equation in the cross-flow plane. Therefore, if we write the velocity potential in the form

$$Ux + \Phi - Uzh'(x) \quad , \qquad (2\text{-}2)$$

Φ will be given by the real part of an analytic function $W(Z)$ where $Z = y + iz$ and W will be determined to within an additive function of x by the boundary conditions. The additive function of x can be determined by considering the flow at a large distance, but this is not necessary for the present calculations.

The conditions to be satisfied on the wing and at infinity are that the wing is a stream surface, i.e.

$$\frac{\partial \Phi}{\partial z} = 0 \qquad \text{on} \qquad z = 0 \tag{2-3}$$

and that the disturbances decay at infinity, i.e.

$$\Phi \sim Uzh'(x) \qquad \text{as} \qquad |Z| \to \infty \quad . \tag{2-4}$$

Following Smith[1] the complex velocity potential can be defined with the aid of the conformal transformation

$$Z^{*2} = Z^2 - s^2 \quad , \tag{2-5}$$

where $s = s(x)$ is the local semispan of the wing. This transformation takes the wing cross-section into a slit on the imaginary axis, as shown in Fig.2b. The complex velocity potential W can now be defined by the equation

$$\frac{dW}{dZ^*} = -ih'(x)U + \frac{\Gamma}{2\pi i}\left(\frac{1}{Z^* - Z_v^*} - \frac{1}{Z^* + \bar{Z}_v^*}\right)$$

$$- \frac{1}{2\pi i}\int_{\Delta\Phi_0}^{\Gamma}\left(\frac{1}{Z^* - Z_c^*} - \frac{1}{Z^* + \bar{Z}_c^*}\right) d\Delta\Phi \quad , \tag{2-6}$$

which, by symmetry, will satisfy the boundary condition on the image of the wing in the Z^*-plane. Since the transformation leaves the plane unchanged at infinity, equation (2-6) will also satisfy the second boundary condition (2-4).

Equation (2-6) defines the complex conjugate of the velocity in the transformed plane due to the free stream component, together with the isolated vortex and its image in the imaginary axis and the vortex sheet and its image in the

imaginary axis. In the right-hand half-plane the isolated vortex of strength Γ is at the point Z_v^* and the circulation at a current point on the vortex sheet, Z_c^*, is $\Delta\Phi$, which varies from $\Delta\Phi_0$ at the leading edge to Γ at the free end of the sheet.

2.2 Boundary conditions on the sheet

The position and strength of both the isolated vortex and the sheet remain to be determined in such a way that the velocity field defined by (2-6) satisfies the Kutta condition at the leading edge, the boundary conditions on the sheet and the boundary conditions on the isolated vortex.

The Kutta condition requires that the velocity should be finite at the leading edge. Since this edge corresponds to a singular point of the transformation, (2-5), the Kutta condition implies that there must be a stagnation point at the image of the leading edge in the transformed plane,

$$\frac{dW}{dZ^*} = 0 \qquad \text{at} \qquad Z^* = 0 \quad . \tag{2-7}$$

The boundary conditions on the sheet are obtained in a general form in Appendix A and then specialised for the particular coordinate system used here. The coordinate system chosen is shown in Fig.2a, and it uses polar coordinates (R,Θ) centred on the isolated vortex with Θ measured from the line joining the vortex to the leading edge. Basing the coordinates on the position of the isolated vortex means that the shape of any length of sheet can be described by a single-valued function $R(x,\Theta)$. Smith[1] used a similar system in the transformed plane but this leads to complicated expressions for the streamwise derivatives. Barsby[6] and Jones[7] use the intrinsic coordinates (ψ,σ) defining the vortex sheet by means of the angle of the tangent ψ as a function of the arc length σ. This system can also be used for any length of sheet, although in practice there can be numerical difficulties in fixing the position of a longer sheet, since any change in ψ close to the leading edge will affect all the subsequent points on the sheet. The intrinsic coordinate system was however able to handle the distorted sheet shapes found by Barsby[6] for conical flows at low incidences. Such a coordinate system might also be more suited to the non-conical wing whose incidence decreases in the streamwise direction (see section 4.3).

In terms of the polar coordinates the boundary conditions on the sheet can be written as (see Appendix A):

$$\frac{\partial R(x,\Theta)}{\partial x} = -\operatorname{cosec}\phi\left(\frac{v_n}{U} + p'(x)\sin\psi - (q'(x) - h'(x))\cos\psi - R(x,\Theta)\gamma'(x)\cos\phi\right) \qquad (2\text{-}8)$$

for the stream surface condition, and for the pressure continuity condition

$$\frac{\partial \Delta\Phi(x,\Theta)}{\partial x} = -\operatorname{cosec}\phi\,\Delta v_t\left(\frac{v_n}{U}\cos\phi + \frac{v_{t_m}}{U}\sin\phi - p'(x)\cos(\Theta + \gamma(x)) - (q'(x) - h'(x))\sin(\Theta + \gamma(x)) - R(x,\Theta)\gamma'(x)\right) . \qquad (2\text{-}9)$$

The partial derivatives on the left-hand side denote differentiation along lines of constant Θ on the vortex sheet and the primes denote differentiation with respect to x. The angles ϕ, ψ and γ are defined in Fig.2a, and p and q are the real and imaginary components of the vortex position Z_v. The tangential component of the velocity at a point on the sheet is discontinuous and v_{t_m} represents the mean tangential component in the cross-flow plane whilst Δv_t denotes the jump in the tangential velocity component across the sheet in the cross-flow plane. v_n is the normal velocity on the sheet in the cross-flow plane measured along the inward normal.

The mean velocity components on the sheet follow from equation (2-2) and from the complex conjugate velocity

$$\frac{dW}{dZ} = v - iw = \frac{dW}{dZ^*}\frac{dZ^*}{dZ} , \qquad (2\text{-}10)$$

evaluated on the sheet.

The velocity components perpendicular to the free stream are therefore v parallel to Oy and $(w - Uh')$ parallel to Oz and so we can substitute for v_n and v_{t_m} in equations (2-8) and (2-9) to obtain

$$\frac{\partial R}{\partial x} = \operatorname{cosec}\phi\left\{\left(\frac{v}{U} - p'\right)\sin\psi - \left(\frac{w}{U} - q'\right)\cos\psi + R\gamma'\cos\phi\right\} \qquad (2\text{-}11)$$

and

$$\frac{\partial \Delta\Phi}{\partial x} = -\operatorname{cosec}\phi\,\Delta v_t\left\{\left(\frac{v}{U} - p'\right)\cos(\Theta + \gamma) + \left(\frac{w}{U} - q'\right)\sin(\Theta + \gamma) - R\gamma'\right\} \quad . \qquad \ldots\ldots \quad (2\text{-}12)$$

It is this form of the equations that is used for the numerical calculation.

The singular integral involved in evaluating (2-6) on the sheet must be treated as a Cauchy Principal Value integral in order to obtain the mean velocity. The part of the integral involving the singularity can therefore be written as

$$\int_0^{Z_E^*} \frac{1}{Z^* - Z_c^*}\frac{d\Delta\Phi}{dZ_c^*}\,dZ_c^* = -\int_0^{Z_E^*} \frac{\dfrac{d\Delta\Phi}{dZ^*} - \dfrac{d\Delta\Phi}{dZ_c^*}}{Z^* - Z_c^*}\,dZ_c^*$$

$$- \frac{d\Delta\Phi}{dZ^*}\ln\left(\frac{(Z_E^* - Z^*)}{Z^*}\right) \quad , \qquad (2\text{-}13)$$

where Z_E^* is the value of Z^* at the free end of the vortex sheet. In this form the singularity has been dealt with analytically and the integral remaining on the right-hand side of (2-13) can be evaluated numerically.

The discontinuity in tangential velocity across the sheet arises from the contribution to this integral of the neighbourhood of the singular point and is given by

$$\Delta v_t = \frac{\partial \Delta\Phi}{\partial \sigma} \quad , \qquad (2\text{-}14)$$

σ being the arc length around the sheet and the partial derivative being evaluated for constant x .

2.3 The zero-force condition

Because the inner part of the vortex sheet has been replaced by an isolated vortex, the pressure continuity condition (2-12) is violated. It is replaced,

as in Ref.1, by the requirement that the total force acting on each isolated vortex and the cut joining it to the end of the finite part of the sheet should vanish. The formulation of this condition closely follows that of Smith[3] but differences arise since the wings considered here have lengthwise camber.

The force per unit length on the isolated vortex filament is given by the product of $-i\rho\Gamma$ and the velocity normal to the vortex induced by the rest of the flow. The dominant terms in this normal velocity are those due to the velocity in the cross-flow plane and a contribution due to the fact that the line vortex is inclined to the free stream. The first of these contributions follows from the velocity potential (2-2) with the contribution from the vortex itself deducted. By equations (2-1) and (2-2) this term is

$$\lim_{Z\to Z_v}\left\{\frac{\partial\Phi}{\partial y'}+i\frac{\partial}{\partial z'}\left(\Phi-Uzh'(x)\right)-\overline{\frac{\Gamma}{2\pi i}\frac{1}{Z-Z_v}}\right\}$$

$$=\lim_{Z\to Z_v}\left\{\overline{\frac{dW}{dZ}-\frac{\Gamma}{2\pi i}\frac{1}{Z-Z_v}}\right\}-iUh'(x)\quad,\tag{2-15}$$

where the bar denotes the complex conjugate. The velocity component due to the inclination of the vortex filament to the free stream is given by

$$-U\frac{d}{dx}\left(y_v'+iz_v'\right)=-U\frac{dZ_v}{dx}+iUh'(x)\tag{2-16}$$

where we have again used equation (2-1). The force per unit length on the cut, due to the difference in pressure across it, follows immediately from Ref.3 and is given by

$$i\rho U(Z_v-Z_E)\frac{d\Gamma}{dx}\quad.\tag{2-17}$$

Combining this with the expressions (2-15) and (2-16) we find the zero-force condition:

$$\left(\overline{Z_v-Z_E}\right)\frac{d\Gamma}{dx}+\Gamma\frac{d\bar{Z}_v}{dx}=\frac{\Gamma}{U}\lim_{Z\to Z_v}\left(\frac{d}{dZ}\left(W-\frac{\Gamma}{2\pi i}\ln\left(Z-Z_v\right)\right)\right)\quad.\tag{2-18}$$

By using equations (2-5) and (2-6) the right-hand side of this equation can be expressed as

$$\frac{\Gamma}{U}\frac{Z_v}{Z_v^*}\left\{-iUh'(x) - \frac{\Gamma}{2\pi i}\frac{1}{Z_v^* + \bar{Z}_v^*} - \frac{1}{2\pi i}\int_{\Delta\Phi_0}^{\Gamma}\left(\frac{1}{Z_v^* - Z_c^*} - \frac{1}{Z_v^* + \bar{Z}_c^*}\right)d\Delta\Phi\right.$$

$$\left. + \lim_{Z\to Z_v}\left(\frac{\Gamma}{2\pi i}\frac{d}{dZ^*}\ln\left(\frac{Z^* - Z_v^*}{Z - Z_v}\right)\right)\right\} ,$$

and evaluating the limit by equation (2-5) we find that the zero-force condition can be written

$$\left(\frac{}{Z_v - Z_E}\right)\frac{d\Gamma}{dx} + \Gamma\frac{d\bar{Z}_v}{dx} = \frac{\Gamma}{U}\frac{Z_v}{Z_v^*}\left\{-iUh'(x)\right.$$

$$- \frac{\Gamma}{2\pi i}\left(\frac{s^2}{2Z_v^2 Z_v^*} + \frac{1}{Z_v^* + \bar{Z}_v^*}\right)$$

$$\left. - \frac{1}{2\pi i}\int_{\Delta\Phi_0}^{\Gamma}\left(\frac{1}{Z_v^* - Z_c^*} - \frac{1}{Z_v^* + \bar{Z}_c^*}\right)d\Delta\Phi\right\} . \quad (2\text{-}19)$$

It can easily be checked that this expression agrees with that given in Ref.3 if the terms involving the vortex sheet are omitted and $h'(x)$ is replaced by the uniform angle of incidence, α .

3 NUMERICAL METHOD

The boundary conditions given by equations (2-11), (2-12) and (2-19) can be regarded as a set of ordinary differential equations which can be integrated with respect to x to follow the evolution of the vortex sheet along lines of constant Θ . The initial conditions required for this integration are provided by the known conical solutions since we can assume that close to the apex the wing is approximately conical.

The streamwise integration is carried out by using a backward-difference formula which leads to the solution of a set of implicit equations at each

streamwise station. In the cross-flow plane the vortex sheet is represented numerically by its strength and position at a finite number of points and the integral terms involved in the velocity field calculations are approximated using the trapezium rule.

3.1 Finite-difference formulation

The vortex sheet shape is defined in terms of the coordinates of the isolated vortex and the values of the polar distance R_i from this point to n points on the sheet at fixed values of the polar angle Θ_i. The circulation on the sheet is defined by that of the isolated vortex, Γ, which fixes the value at the free end of the sheet, and the circulation per unit length of the sheet, $\left(\frac{\partial \Delta\Phi}{\partial \sigma}\right)_i$, evaluated at the leading edge, $\Theta = 0$, and at the n points defining the sheet.

The flow field in the cross-flow plane is defined by equation (2-6) in terms of the basic non-dimensional variables making up the vector quantity

$$\underline{Y} = \left(R_1/s, \ldots, R_n/s, \frac{1}{AU}\left(\frac{\partial \Delta\Phi}{\partial \sigma}\right)_0, \ldots, \frac{1}{AU}\left(\frac{\partial \Delta\Phi}{\partial \sigma}\right)_n, p/s, q/s \right) \qquad (3\text{-}1)$$

where $A(x)$ is the 'local aspect ratio' defined by

$$A(x) = 2s^2 \Big/ \int_0^x s\,dx \quad . \qquad (3\text{-}2)$$

In this form $A(x)$ provides a generalisation of the sweepback parameter $K = s/x$ which was used for the conical flow calculations. s/x itself is not appropriate because it conflicts with the form of the similarity solutions (see section 4.1) and $s'(x)$ cannot be used for wings for which $s'(x)$ vanishes.

For any given value of the vector $\underline{Y}$ the circulation Γ can be calculated from the Kutta condition, equation (2-7). The velocity at any point in the cross-flow plane then follows from equation (2-6), and the circulation on the sheet is given by

$$\Delta\Phi_i = \Delta\Phi_{i+1} + \int_{\sigma_{i+1}}^{\sigma_i} \frac{\partial \Delta\Phi}{\partial \sigma}\, d\sigma \qquad (3\text{-}3)$$

using $\Delta\Phi_n = \Gamma$. The integration is performed by applying the trapezium rule either to

$$\int_{\Theta_{i+1}}^{\Theta_i} \frac{\partial \Delta\Phi}{\partial \sigma} \frac{d\sigma}{d\Theta}\, d\Theta = \int_{\Theta_{i+1}}^{\Theta_i} \frac{\partial \Delta\Phi}{\partial \sigma} \frac{R}{\sin \phi}\, d\Theta \qquad (3\text{-}4)$$

or else, if ϕ is small, to

$$\int_{R_{i+1}}^{R_i} \frac{\partial \Delta\Phi}{\partial \sigma} \frac{d\sigma}{dR}\, dR = \int_{R_{i+1}}^{R_i} \frac{\partial \Delta\Phi}{\partial \sigma} \sec \phi\, dR \quad . \qquad (3\text{-}5)$$

Since R_i and $(\partial\Delta\Phi/\partial\sigma)_i$ are evaluated at fixed values of $\Theta = \Theta_i$, $\underline{Y}$ will be a function of x alone and, for conical flow, because its components have been appropriately non-dimensionalised, $\underline{Y}$ will be constant. If $\underline{Y}$ is known at equally spaced stations, δx apart, upstream of x , then its derivative $\underline{Y}'(x)$ can be approximated in terms of $Y(x)$ using the backward-difference formula

$$\underline{Y}'(x) = \frac{1}{6\delta x}\left(11\underline{Y}(x) - 18\underline{Y}(x - \delta x) + 9\underline{Y}(x - 2\delta x) - 2\underline{Y}(x - 3\delta x)\right) \quad , \qquad \ldots\ldots (3\text{-}6)$$

where terms of relative order $(\delta x)^3$ have been neglected.

By using this equation to replace the derivatives occurring on the left-hand sides, the boundary conditions (2-11) and (2-12) and the force condition (2-19) can be written as a set of non-linear equations for the unknown elements of the vector $\underline{Y}(x)$. The normal velocity condition, equation (2-11), is applied at the n pivotal points defining the sheet, and the pressure condition, equation (2-12), is applied at these points and at the leading edge. The tangential velocities above and below the leading edge of the wing required for this last condition are not calculated directly but are found by extrapolation from the values calculated at the first pivotal point and at a supplementary point midway between the leading edge and the first pivotal point.

The boundary conditions together give a set of $2n + 3$ non-linear equations to solve for the $2n + 3$ basic variables involved in $\underline{Y}(x)$. For any vector $\underline{Y}$ we can therefore calculate the vector $\underline{F}(\underline{Y})$ whose components consist of the residual values of each of these equations, so that the problem at each streamwise station can be written in the form

$$\underline{F}(\underline{Y}) = 0 \quad . \tag{3-7}$$

The terms involved in these residual equations are non-dimensionalised in such a way as to ensure that for the conical flows, and for the self-similar flows discussed in section 4.1, their dependence on x is eliminated. The normal velocity equations which are proportional to $\frac{\partial R}{\partial x}$ are therefore divided by A , the pressure continuity equations, proportional to $\frac{\partial \Delta\Phi}{\partial x}$, are divided by UA^2 and the zero-force equation, proportional to $Z_v \frac{d\Gamma}{dx}$, is divided by $UA^2 s$.

3.2 Iterative scheme

In order to solve equation (3-7), we suppose that we have an approximation $\underline{Y}_s$ to the solution. Then for $\underline{Y}$ near $\underline{Y}_s$ we can write

$$\underline{F}(\underline{Y}) = \underline{F}(\underline{Y}_s) + J_s(\underline{Y} - \underline{Y}_s) + \ldots \quad , \tag{3-8}$$

where J_s is the Jacobian matrix, $\left[\frac{\partial F_i}{\partial Y_j}\right]$, evaluated at $\underline{Y} = \underline{Y}_s$, consisting of the partial derivatives of the components of the residual vector with respect to the components of the vector $\underline{Y}$.

If we assume that $\underline{F}$ has a locally-linear behaviour then we can neglect the higher order terms in this expansion to obtain a further approximation $\underline{Y}_{s+1}$ to the solution of (3-7):

$$\underline{Y}_{s+1} = \underline{Y}_s - J_s^{-1}\underline{F}(\underline{Y}_s) \quad . \tag{3-9}$$

This is the multi-dimensional extension of Newton's iterative method. This iterative procedure has been applied to other flows with leading-edge separation by Pullin[5] and Barsby[6] in their work on conical flows.

The initial approximation for the iterative procedure, (3-9), is obtained by extrapolation from upstream values and the iteration is continued until the sum of the squares of the residuals is less than a predetermined value. It was

generally found to be advantageous to use three upstream values for the initial extrapolation since this reduced the number of iterations required to obtain a converged solution.

The Jacobian matrix is evaluated by numerical differentiation using the approximation

$$\frac{\partial \underline{F}}{\partial Y_i} \simeq \frac{\underline{F}\left(Y_1, \ldots, Y_i + \varepsilon Y_i, \ldots, Y_{2n+3}\right) - \underline{F}(Y_1 \ldots, Y_{2n+3})}{\varepsilon Y_i} \quad \ldots\ldots (3\text{-}10)$$

The iterative method does not seem to be particularly sensitive to the choice of the interval ε, but that used here is $\varepsilon = 10^{-6}$. The calculation of the Jacobian matrix involves a large number of velocity field evaluations and is therefore a lengthy calculation. As Barsby[6] found for the conical solutions, the iterative process can be speeded up very significantly by using the same Jacobian matrix for several consecutive iterations. This slows the rate of convergence down from second to first order, but the overall computing time is greatly reduced by the need for fewer calculations of the Jacobian matrix. The rate of convergence was measured by the ratio of the sum of the squares of the residuals of successive approximations and a new Jacobian was calculated only when this factor became larger than 0.4, this value being a compromise, avoiding both an excessive number of iterations and an excessive number of calculations of the Jacobian. In practice it was found that the same matrix could even be used economically to produce converged solutions at a number of streamwise stations. A few calculations were made to check the effect of step size. As a result a step size of the order of 5% of the wing chord was chosen. For wings with more rapid variations in shape, smaller steps would be required.

The streamwise integration process requires a suitable starting solution and this is provided by the known conical solutions which can be applied close to the apex where the flow can be regarded as conical. The conical solution is provided as data for the calculation. If this conical solution is not sufficiently accurate then difficulties could be experienced over the convergence of the solution as the integration proceeds downstream. The starting data can therefore be refined if necessary by using the iterative procedure described above. In this case, since $\underline{Y}$ is independent of x for conical flow, the derivatives required for insertion in the governing equations can now be determined from

$$\underline{Y}'(x) = 0 \qquad (3\text{-}11)$$

instead of the backward-difference formula (3-6).

4 APPLICATION TO NON-CONICAL WINGS

4.1 Self-similar solutions - validation of the method

In the previous section it was pointed out that the basic vector $\underline{Y}$ is independent of x for conical wings. In fact these conical solutions are part of a wider family of wings for which such self-similar solutions exist. This family of wings was examined by Smith[13] who found that for wings defined by

$$\left.\begin{aligned} s(x) &= ax^{\nu} \\ h(x) &= bx^{\nu} \end{aligned}\right\} \qquad (4\text{-}1)$$

where a, b and ν are constants, the vortex sheet shape will be similar in all cross-flow planes, with its length scale being proportional to $s(x)$. Also the vortex density on the sheet depends on x through $s'(x)$ alone, and so with the non-dimensionalisation chosen in (3-1) we can see from equations (3-2) and (4-1) that $\underline{Y}$ will be independent of x. The conical solutions already referred to can now be seen to be recovered for the particular choice $\nu = 1$ in equations (4-1).

The existence of these solutions provides a useful check for the numerical method outlined in the previous section. Starting from one of these known solutions the definition of the local semispan and incidence can be changed to correspond to another member of the family defined by equation (4-1). If the flow were attached, according to slender-body theory the cross flow would depend only on the local semispan and incidence, i.e. it would change at once to that appropriate to the second member of the family. The presence of circulation shed further upstream modifies this, but as the integration is carried downstream away from this changeover point the influence of the original solution can be expected to decrease and the behaviour to approach that of the corresponding new similarity solution. This was indeed found to occur and Fig.3 illustrates the behaviour of the total circulation for one such wing. For $x \leqslant 0.01$ the wing shape corresponds to a similarity parameter $\nu = 0.95$ in equation (4-1). Downstream of this point the wing shape corresponds to a similarity parameter $\nu = 0.90$ with $s(x)$ and $h(x)$ defined so that they are

continuous, although their derivatives are discontinuous, at $x = 0.01$. There was a tendency for oscillation to occur about the limiting downstream solution, but this behaviour was thought to be caused by the discontinuity which occurs in the local angles of incidence and leading-edge sweep at the change from the initial planform, combined with the high-order difference formula used for the downstream integration. For the remaining wings which have been examined the change from the conical starting configuration to the wing being studied was achieved more smoothly and no such oscillations were observed in the solutions.

4.2 Plane wings with curved leading edges

In the family of similar solutions[13], the shape of the planform is simply related to the lengthwise camber, by equation (4-1). The effects of planform changes can now be considered independently. As an example a wing designated II in Ref.3 is chosen. Its planform is shown in Fig.4 and its leading edge consists of a straight section followed by a parabolic section joining smoothly onto a portion of the wing with streamwise edges, the wing being defined by

$$\left.\begin{aligned} s(x) &= 0.25x \quad , && 0 \leqslant x \leqslant 1.1 \\ s(x) &= -0.125x^2 + 0.525x - 0.15125 \quad , && 1.1 < x \leqslant 2.1 \\ s(x) &= 0.4 \quad , && x > 2.1 \end{aligned}\right\}$$

and

$$h(x) = 0.1x \quad , \qquad \ldots\ldots \text{(4-2)}$$

so that the wing is at an angle of incidence of 0.1 radians.

Using the isolated vortex model, Smith[3] found that as his calculation proceeded downstream in the region of increasing leading-edge sweep, the strength of the isolated vortex decreased, implying that vorticity of the opposite sign was being shed from the leading edge. It was not clear at the time whether this was realistic or was due to the inadequate model of the separated flow. It can be seen from Fig.5, in which the total circulation on the sheet and in the isolated vortex is plotted against the downstream distance, that a similar reduction in the circulation still occurs when the outer part of the sheet is represented in the model. In fact the agreement in the total circulation between this method and the isolated vortex model is remarkably close.

The vortex sheet strength is plotted against the angular coordinate on the sheet at several streamwise stations in Fig.6. As the leading-edge sweep increases, the vorticity being shed from the leading edge decreases and becomes negative. This region where negative vorticity is being shed corresponds to that over which the total circulation is decreasing. Beyond about $x = 2.5$ the vorticity being shed from the leading edge becomes positive and the circulation begins to increase. The region of negative vorticity can be seen to be convected around the vortex sheet as the distance downstream increases.

The corresponding vortex sheet shapes are plotted in Fig.7 (note false origin) and it is worth noting that this region of negative vorticity on the sheet appears to have no noticeable effect on the behaviour of the sheet, which varies smoothly in the streamwise direction. This figure also shows that the position of the isolated vortex is changed significantly by the inclusion of the outer part of the vortex sheet. For the conical solution the isolated vortex model predicts a vortex which is too far outboard, whereas further downstream it predicts a vortex which is too close to the wing.

4.3 Wings with lengthwise camber

A wing with delta planform was chosen to study the effects of lengthwise camber. Results are presented for the wing defined by

$$\left.\begin{aligned} s(x) &= 0.25x \quad , \\ h(x) &= 0.2x \quad , \qquad 0 \leqslant x \leqslant 1 \\ \text{and} \quad h(x) &= 0.1(4x - x^2 - 1) \quad , \quad 1 < x \leqslant 2 \quad . \end{aligned}\right\} \quad (4\text{-}3)$$

These equations define a wing which is initially conical as far as $x = 1$ with an angle of incidence of 0.2 radians downstream of which the local angle of incidence decreases linearly to zero at $x = 2$ as shown in Fig.8.

The vortex sheet strength is shown in Fig.9. As the local incidence is reduced, the vorticity being shed from the leading edge decreases and becomes negative. The absolute value of this negative vorticity is large in comparison with the values elsewhere on the sheet and in comparison with Fig.6. The corresponding vortex sheet shapes are shown in Fig.10 from which we can see that the change in the sign of the vorticity on the sheet is associated with a drastic change in its shape. As negative vorticity is shed from the leading

edge the sheet begins to bulge towards the lower surface of the wing whilst the vorticity on the remainder of the sheet decreases so that it carries very little circulation. For this configuration the negative vorticity does not appear to be convected around the sheet but the negative circulation builds up near the leading edge. The calculation could not be taken any further than about $x = 1.8$ because of the difficulty over the representation of this distorted sheet. This difficulty arises because the vortex sheet is defined in terms of polar coordinates based on the isolated vortex position for fixed polar angles. It is not possible therefore to represent a sheet which passes below the extension of the line joining the vortex to the leading edge. This deformation of the sheet can be interpreted as the beginning of the new vortex system which must form on the underside of the wing as the effective local incidence changes sign, although this method does not as it stands provide an adequate representation of the two vortex systems. It would be expected that this new vortex would be formed before the point at which the geometric incidence vanishes, since the vorticity generated upstream of this point creates a downwash at the leading edge thereby reducing the effective incidence. The calculation reflects this behaviour.

In an attempt to quantify this effect some wind tunnel tests were carried out on a delta wing cambered along the wing centre line. This investigation is discussed in Appendix B, where the results obtained are compared with those of previous studies[14-16].

5 CONCLUSIONS

A vortex-sheet representation of flow which separates from the leading edge of a slender wing has been extended to non-conical flow. The boundary conditions which determine the shape and strength of the vortices are formulated as ordinary differential equations in terms of the streamwise coordinate. An implicit, backward-difference scheme for the solution of these equations, starting from a known conical solution, is formulated. The method is shown to be stable and to be capable of producing known solutions accurately.

Solutions are presented for two examples: a plane wing with a curved leading edge and a delta wing with negative longitudinal camber. In each case the method predicts the shedding of circulation of the reversed sign from some part of the leading edge. On the plane wing, this negative circulation is convected smoothly into the core of the vortex: the shape of the vortex sheet

is smooth, as is found experimentally for plane wings at incidence. On the cambered wing, the negative circulation appears to build up near the leading edge, producing a distortion of the shape of the sheet which suggests that a vortex of the opposite sense of rotation is about to form below the lower surface. The coordinate system chosen to describe the vortex sheet is unable to describe the further development of the sheet. Some new experimental evidence is presented to elucidate the flow over the cambered wing.

Acknowledgment

The assistance of N.C. Lambourne (RAE) and D.W. Bryer (NPL) in making their flow photographs available is gratefully acknowledged.

Appendix A

THE VORTEX-SHEET BOUNDARY CONDITIONS

The boundary conditions which must be applied on the vortex sheet follow from the requirements that it should be a stream surface of the three-dimensional flow and that it can sustain no pressure discontinuity. We shall derive these conditions in terms of a set of general coordinates defined on the vortex sheet Σ, and then interpret them in terms of the polar coordinates used for the numerical calculations. The derivation of the general equations is based on that put forward by Smith[4].

We can define the parametric surface coordinates ξ and η on Σ such that ξ is measured in the direction of the free stream and η is measured in the cross-flow plane, ξ = constant. Any point on the vortex sheet can therefore be expressed in terms of the parametric coordinates ξ and η, and the shape of the vortex sheet will be defined as a function of these two variables. As an example of these general coordinates the numerical method given in this paper uses polar coordinates (R,Θ) in the cross-flow plane, as defined by Fig.2a, so that $\xi = x$, the downstream distance and $\eta = \Theta$, the polar angle. The shape of the vortex sheet can now be defined by the polar distance $R = R(x,\Theta)$.

Let $\underline{i}$ be the unit vector parallel to the free stream and let $\underline{a}$ and $\underline{b}$ be unit vectors in the tangent plane at a point on the vortex sheet such that $\underline{a}$ is in the direction of η = constant with ξ increasing and $\underline{b}$ is in the direction of ξ = constant with η increasing. The vector $\underline{a} \times \underline{b}$ is therefore normal to the three-dimensional surface Σ, and the unit vector normal to the trace of Σ in the cross-flow plane is given by $\underline{n} = \underline{i} \times \underline{b}$. The vectors $(\underline{i},\underline{b},\underline{n})$ therefore form a right-handed orthogonal triad of unit vectors as shown in Fig.11.

The velocity is discontinuous across Σ, but the value it takes as Σ is approached from one side can be written as

$$\underline{v} = (U + u)\underline{i} + v_t\underline{b} + v_n\underline{n} \quad ; \qquad (A\text{-}1)$$

and we assume that the components of the disturbance velocity (u,v_t,v_n) are small in comparison with the free stream velocity U.

We can also resolve the vector $\underline{a}$ into three orthogonal components to obtain

$$\underline{a} = (\underline{a} \cdot \underline{i})\underline{i} + (\underline{a} \cdot \underline{b})\underline{b} + (\underline{a} \cdot \underline{n})\underline{n} \quad , \tag{A-2}$$

so that

$$\underline{a} \times \underline{b} = (\underline{a} \cdot \underline{i})\underline{n} - (\underline{a} \cdot \underline{n})\underline{i} \quad . \tag{A-3}$$

The requirement that Σ should be a stream surface is

$$\underline{v} \cdot (\underline{a} \times \underline{b}) = 0 \quad , \tag{A-4}$$

which with the aid of equations (A-1) and (A-3) gives

$$\frac{v_n}{U} = \frac{\underline{a} \cdot \underline{n}}{\underline{a} \cdot \underline{i}} \left(1 + \frac{u}{U}\right) \simeq \frac{\underline{a} \cdot \underline{n}}{\underline{a} \cdot \underline{i}} \tag{A-5}$$

since we can neglect u in comparison with U, and this condition then gives the same value for v_n on both sides of Σ.

We associate the suffices 1 and 2 with the two sides of the surface Σ such that the normal vector $\underline{n}$ points towards side 1. The second boundary condition requires that the static pressure is continuous across Σ and so, if we assume that the total pressure is the same on both sides of Σ and that the density is a function of the pressure alone, the speed must be continuous across the sheet. This condition is therefore

$$\Delta\left((U + u)^2 + v_t^2 + v_n^2\right) = 0 \quad , \tag{A-6}$$

where the difference operator Δ denotes the value on side 1 of the sheet minus that on side 2. By retaining the second order term in equation (A-5) we find that

$$\Delta v_n \simeq \frac{v_n}{U} \Delta u \quad ,$$

so that we can neglect Δv_n in comparison with Δu. We can also neglect u in comparison with U so that equation (A-6) becomes

$$U\Delta u + v_{t_m} \Delta v_t = 0 \qquad \text{(A-7)}$$

where $v_{t_m} = \frac{1}{2}(v_{t_1} + v_{t_2})$ is the mean tangential velocity in the cross-flow plane. Again neglecting the term involving Δv_n we can use equations (A-1) and (A-2) to obtain

$$\Delta u = \Delta \underline{v} \cdot \underline{i} = \Delta \underline{v} \cdot \left(\underline{a} - (\underline{a} \cdot \underline{b})\underline{b}\right) \Big/ (\underline{a} \cdot \underline{i}) \quad . \qquad \text{(A-8)}$$

If $g_\xi d\xi$ denotes the arc length along the curve η = constant on Σ due to a small increment $d\xi$ in ξ and $\Phi_1(\xi,\eta)$ denotes the velocity potential on side 1 of Σ, then the velocity component parallel to $\underline{a}$ on side 1 of Σ is given, on the one hand by $\underline{a} \cdot \underline{v}_1$, and on the other by

$$\lim_{d\xi \to 0} \frac{\Phi_1(\xi + d\xi, \eta) - \Phi_1(\xi,\eta)}{g_\xi d\xi} \quad .$$

Therefore

$$\underline{a} \cdot \underline{v}_1 = \frac{1}{g_\xi} \frac{\partial \Phi_1}{\partial \xi} \quad . \qquad \text{(A-9)}$$

The component of the velocity jump parallel to $\underline{a}$ is therefore

$$\underline{a} \cdot \Delta \underline{v} = \frac{1}{g_\xi} \frac{\partial \Delta\Phi}{\partial \xi} \quad . \qquad \text{(A-10)}$$

Also, from equation (A-1) we can see that

$$\underline{b} \cdot \Delta \underline{v} = \Delta v_t \qquad \text{(A-11)}$$

and so combining these results with equations (A-7) and (A-8) the second boundary condition on Σ becomes

$$\frac{1}{g_\xi} \frac{\partial \Delta\Phi}{\partial \xi} = \Delta v_t \left(\underline{a} \cdot \underline{b} - \underline{a} \cdot \underline{i} \frac{v_{t_m}}{U} \right) \quad . \qquad \text{(A-12)}$$

To interpret the boundary conditions (A-5) and (A-12) in terms of the polar coordinates used here (see Fig.2a) we observe that $\xi = x$, $\eta = \Theta$ and in terms of the cartesian axes $O'xy'z'$ centred on the apex of the wing

$$\underline{i} = (1, 0, 0)$$

$$\underline{b} = (0, \cos\psi, \sin\psi)$$

and

$$\underline{a} = (a_x, a_y, a_z) \quad . \tag{A-13}$$

A general point on the vortex sheet can be written as

$$\underline{P}(x,\Theta) = \Big(x,\ p(x) + R(x,\Theta)\sin(\Theta + \gamma(x)),\ q(x) - h(x) - R(x,\Theta)\cos(\Theta + \gamma(x))\Big) \quad , \tag{A-14}$$

and since on the surface

$$d\underline{P} = \frac{\partial \underline{P}}{\partial x}dx + \frac{\partial \underline{P}}{\partial \Theta}d\Theta = \underline{a}g_x dx + \underline{b}g_\Theta d\Theta \tag{A-15}$$

it follows that

$$g_x\underline{a} = \Big(1,\ p' + \frac{\partial R}{\partial x}\sin(\Theta + \gamma) + R\gamma'\cos(\Theta + \gamma),\ q' - h' - \frac{\partial R}{\partial x}\cos(\Theta + \gamma) + R\gamma'\sin(\Theta + \gamma)\Big) \quad . \tag{A-16}$$

From Fig.2a we can see that $\Theta + \gamma - \psi = (\pi/2) - \phi$ and using this together with equations (A-13) and (A-16) we find that

$$\frac{\underline{a}\cdot\underline{n}}{\underline{a}\cdot\underline{i}} = \frac{\underline{a}\cdot(\underline{b}\times\underline{i})}{\underline{a}\cdot\underline{i}} = p'\sin\psi - (q' - h')\cos\psi + \frac{\partial R}{\partial x}\sin\phi - R\gamma'\cos\phi \quad \ldots\ldots \text{(A-17)}$$

so that the normal velocity condition (A-5) becomes

$$\frac{\partial R}{\partial x} = -\operatorname{cosec}\phi\left\{\frac{v_n}{U} + p'\sin\psi - (q' - h')\cos\psi - R\gamma'\cos\phi\right\} \quad . \tag{A-18}$$

Similarly we can combine equations (A-12), (A-13) and (A-16) together with (A-18) to obtain the pressure continuity condition

$$\frac{\partial \Delta\Phi}{\partial x} = -\operatorname{cosec}\,\phi\,\Delta v_t\left\{\frac{v_n}{U}\cos\phi + \frac{v_{t_m}}{U}\sin\phi - p'\cos(\Theta+\gamma) - (q'-h')\sin(\Theta+\gamma) - R\gamma'\right\} \quad . \quad \text{(A-19)}$$

Appendix B

EXPERIMENTAL INVESTIGATION OF A WING WITH LENGTHWISE CAMBER

Visualisation of the flow over delta wings with lengthwise camber has been reported by Jones[14], Nangia and Hancock[15], and Snyder[16]. Jones[14], in describing some preliminary experiments by N.C. Lambourne and D.W. Bryer, showed photographs of flow in a water tunnel past a thin delta wing with lengthwise camber, at an attitude such that the plane containing the apex and the trailing edge is parallel to the undisturbed flow. Although the flow over a delta wing involves vortices in pairs, one from each leading edge, it is less confusing to refer only to the vortex or vortices from one of the leading edges. It is also convenient to refer to the concave and convex sides of the wing. For the published water-tunnel photographs, the vortex on the concave side was made visible by the introduction of a stream of small bubbles of air. There is a strong tendency, because of buoyancy, for bubbles to be drawn to the low-pressure region along the axis of a vortex and, if the concentration is sufficient, to form a core of air along the vortex axis. This is what appears to be happening in the published photographs.

When this core of air approaches the streamwise station at which the local geometric incidence vanishes, it appears to pass outboard, round the leading edge, and continue downstream on the opposite (convex) side of the wing. This suggests at first sight that, in the absence of the core of air, the vortex formed over the forward part of the wing is convected round the leading edge, near the station of zero local incidence, to become the vortex on the new leeside. Such an interpretation is not consistent with the findings of Snyder[16], who followed the paths of the vortex cores by injecting steam into them. He describes a vortex which forms on the concave side of the wing near the apex and continues downstream on the same side of the wing, past the station of zero incidence, to the trailing edge; and a second vortex which forms on the convex side of the wing near the station of zero local incidence and continues on the same side of the wing to the trailing edge. Nangia and Hancock[15] did not find the second vortex when the wing was at this same attitude, but describe the vortex on the concave side crossing the leading edge when the inclination of the apex to the stream is somewhat less.

The present calculations are interpreted in section 4 as indicating that a second vortex of opposite sign forms a short distance upstream of the station

of zero local incidence. Certainly the calculations give no indication that the vortex formed over the forward part of the wing is convected outboard round the leading edge. Unfortunately they could not be carried far enough to reveal just how the flow develops. In order to provide a basis for modelling the flow further downstream, a simple flow visualisation experiment was carried out in the No.1 $11\frac{1}{2}$ft × $8\frac{1}{2}$ft low-speed wind tunnel.

A thin delta wing of aspect ratio 1, about 0.96m in length, with sufficient lengthwise camber of approximately parabolic form to give a difference in the local angle of incidence of 30° between the apex and the trailing edge, was mounted in the tunnel on a strut attached to a stiffening member mounted along the wing centre line. The incidence of the model was controlled by bracing wires attached to the wing at about one-quarter of the chord from the apex. The flow at various angles of overall incidence was investigated by surface oil-flow, using a suspension of lamp black in paraffin oil, by the injection of 'smoke' formed from paraffin, by tufts mounted along the leading edge and by a paper cone attached by a short thread to the tip of a wire, itself supported by a thin rod. This last probe is a sensitive indicator of the location of a vortex, since the cone rotates vigorously when the tip of the wire lies in a vortex core.

With the wing set so that the line joining its apex and trailing edge was aligned with the free stream the vortices shed from the forward part of the wing form over the concave surface. In this case it was possible to follow these vortices all the way back to the trailing edge using the vortex probe. Vortices of the opposite sense could also be found on the convex surface of the wing and followed forward towards an apparent origin at the leading edge, near where the local geometric incidence vanished.

The leading edge of the wing was cut at right-angles to the wing surface so that the cross-sectional shape took the form of a thin rectangle. The tufts consisted of pieces of wool about 10 to 20mm in length and they were attached by one end along the leading edge of the wing. Over the forward part of the wing the tufts were swept upwards (the wing was mounted concave side upwards) by the influence of the vortex above the wing, and over the rear part of the wing the tufts were swept below the wing. Precise measurement of the point at which the tufts switched from above the wing to below the wing was not possible because in this region the tufts were all nearly parallel to the leading edge. It did however occur near the position of zero geometric incidence.

The smoke, produced by a proprietary device marketed for stage use, was introduced at the apex of the wing. The flow field was illuminated by a planar beam of light across the flow. By viewing this plane obliquely, it was possible to see the smoke lying in the vortices formed over the forward part of the wing and, by translating the beam, to follow them back to the trailing edge of the wing. Unfortunately, the contrast was inadequate for photography.

The oil flow on the concave surface of the wing is shown in Fig.12a for the case in which the angle of incidence at the apex was 15°, i.e. the free stream was parallel to the plane containing the apex and the trailing edge. The pronounced lines emanating from the apex are the secondary separation lines at which the flow separates under the primary vortices formed at the apex. The effect of some slight lateral asymmetry can be seen in the behaviour of these lines close to the trailing edge. However these lines indicate the presence of the primary vortices on this side of the wing until well after the station of zero geometric incidence, and therefore until well after the formation of the new vortices on the convex surface. Downstream of the point at which the right-hand separation line crosses the leading edge, outboard flow can still be seen, indicating that the vortex is still on the concave side of the wing. This surface oil flow is therefore entirely consistent with the description of the flow put forward here.

These observations therefore confirm the essential features of Snyder's description of the flow, but the photograph published by Jones[14] remains to be explained. It is thought that the column of air trapped in the core of the upstream vortex is large enough to respond to the pressure gradients in the water flow, rather than to the tangential stresses. As the local angle of incidence of the wing reduces in the streamwise direction, the pressure on the concave surface surrounding the vortex will rise. When a new vortex forms further aft on the convex surface of the wing, a region of low pressure will occur in its core. It is suggested that air from the core of the upstream vortex is driven by this pressure gradient round the leading edge and into the core of the downstream vortex, so that the path of the air does not indicate the path taken by the core of the vortex in the absence of the air.

Confirmation is provided by unpublished photographs made available by Lambourne and Bryer. These were taken at the same time as those published by Jones and are reproduced in Fig.13. For both photographs a filament of dye was introduced upstream of the apex of the model. In Fig.13a, the dye appears

initially to follow both surfaces of the wing. On the concave side it is convected into a vortex formed at the apex and shows the continuation of this well past the station of zero local incidence. The striations which appear in the vortex over the forward part of the wing may arise from the helical pattern of the streamlines inside the vortex. On the convex side the dye shows a second vortex forming near the station of zero local geometric incidence. The dye has apparently followed the convex wing surface until the leading-edge vortex sheet begins to roll up on the convex side, forming a vortex which convects the dye outboard and into itself.

In Fig.13b, the dye is initially confined to a region close to the axis of the vortex formed near the apex. The whole of this filament remains on the concave side until some distance downstream of the station of zero local incidence. Part of the dye is then convected round the leading edge in two distinct filaments which are wrapped round the axis of the vortex on the convex side, remaining some distance away from it. The details of the process by which the dye from the core of the vortex on the concave side finds its way round the leading edge are not clear.

The oil-flow photographs provide an opportunity for a quantitative comparison between the theoretical model and the real flow. In Figs.12b, c and d, the flow on the convex surface of the wing is shown. Over the forward part of the wing the flow is directed outboard near the leading edge and inboard over most of the semi-span. (The disturbance near the front end of the marker tape attached along the centre line is produced by the attachment of the bracing wire.) This is consistent with a pair of vortices lying on the concave side of the wing. Over the rear of the wing, there is a strong outflow some little way inboard of the leading edge, terminating in a secondary separation line, which is usually dark. This secondary separation line is the clearest indication of the presence of the vortex on the convex surface.

Since it is difficult to see where along the leading edge this secondary separation line first appears, the station at which it is a small fixed distance (about 0.15% of the root chord) from the leading edge was measured on the photographs. (NB: The dark border around the wing is part of the wind-tunnel background.) Because of the lateral asymmetry existing in the flow, the right-hand side of the wing was used throughout for consistency. These positions are shown as a function of the geometric angle of incidence of the apex of the wing in Fig.14. These measurements show a remarkably smooth variation, and are clearly related to the position at which the local geometric incidence vanishes.

With one marginal exception, they lie just upstream of this position. Since the vortex on the convex surface must be formed upstream of the station at which the secondary separation is identified, it is concluded that it forms upstream of the station at which the local geometric incidence vanishes.

For comparison, Fig.14 also shows the lengthwise stations at which the numerical solution breaks down, again as a function of the apex incidence of the wing. The breakdown of the calculation is simply a failure of the Newton method (section 3.2) to converge to a solution. The breakdown of this calculation was usually accompanied either by the development of a point of inflection on the sheet or by the shedding of vorticity of the opposite sign from the leading edge, although there were no such features common to all of the cases considered. It has not therefore been possible to identify a single cause of breakdown. However the points shown in Fig.14 have a consistent and reasonably smooth dependence on the apex incidence. In the cases considered here the breakdown occurs before the build up of circulation of the opposite sign over the convex surface which was observed in Fig.10, which suggests that it occurs before the appearance of this new vortex. In this sense, the calculated points in Fig.14 are in a consistent relation to the measured points.

As the apex incidence was increased the breakdown of the numerical calculations was found to occur at increasing local angles of incidence, but no similar trend was observed in the experimental measurements. This difference may be due to the absence of trailing-edge effects in the mathematical model.

SYMBOLS

$\underline{a}$, $\underline{b}$	unit vectors tangential to the vortex sheet - see Appendix A
$A(x)$	local aspect ratio - see equation (2-3)
a, b	constants in equation (4-1)
$\underline{F}(\underline{Y})$	residual values in governing equations - see section 3.1
g_x, g_ξ	arc-length scale factors - see Appendix A
$h(x)$	wing centre line camber
$\underline{i}$	unit vector parallel to free stream
J	Jacobian matrix of $\underline{F}$ with respect to $\underline{Y}$ - see section 3.2
K	$= s/x$
$\underline{n}$	unit vector along inward normal to vortex sheet in cross-flow plane
n	number of points defining vortex sheet
$p(x)$, $q(x)$	horizontal and vertical distance of isolated vortex from wing centre line
$\underline{P}(x,\Theta)$	vector position of a general point on the vortex sheet - see Appendix A
$R(x,\Theta)$	polar distance from isolated vortex
$s(x)$	local semispan
u	component of velocity perturbation parallel to free stream
U	speed of free stream
$\underline{v}$	fluid velocity
v_n	component of velocity along inward normal to vortex sheet in cross-flow plane
v_t	component of velocity tangential to the vortex sheet in the cross-flow plane
v_{t_m}	mean component of tangential velocity in the cross-flow plane
v, w	real and imaginary components of the complex velocity - see equation (2-10)
$W(Z)$	complex velocity potential
y, z	cartesian coordinates in cross-flow plane - see Fig.2a
x, y', z'	cartesian coordinates based on apex - see Fig.1
$\underline{Y}(x)$	vector defining position and strength of the vortex sheet and isolated vortex - see equation (3-1)
Z	$= y + iz$, complex coordinate in cross-flow plane
Z^*	$= (Z^2 - s^2)^{\frac{1}{2}}$, complex coordinate in transformed plane
$\gamma(x)$	see Fig.2a
Γ	circulation about isolated vortex
ϵ	increment used for numerical differentiation

SYMBOLS (concluded)

δx	steplength for streamwise integration
Δ	difference operator across vortex sheet
$\Delta\Phi_0$	total circulation about vortex sheet and isolated vortex
Φ	cross-flow velocity potential
ϕ	angle between radius vector and the tangent to the vortex sheet - see Fig.2a
Θ	polar angle measured about isolated vortex - see Fig.2a
ξ, η	parametric coordinates - see Appendix A
ρ	density
ν	similarity parameter - see section 4.1
σ, ψ	intrinsic sheet coordinates - see Fig.2a
Σ	vortex sheet - see Appendix A

Suffices

c	current position on vortex sheet
E	free end of vortex sheet
i	point on vortex sheet
s	current approximation to solution
v	position of isolated vortex
1, 2	separate sides of vortex sheet

REFERENCES

No.	Author	Title, etc.
1	J.H.B. Smith	Improved calculations of leading-edge separation from slender delta wings. Proc. Roy. Soc. A. 306, 67-90 (1968) RAE Technical Report 66070 (ARC 27897) (1966)
2	C.E. Brown W.H. Michael	On slender delta wings with leading-edge separation. Journ. Aero. Sci., 21, 690-694 and 706 (1954) NACA TN 3430 (1955)
3	J.H.B. Smith	A theory of the separated flow from the curved leading edge of a slender wing. ARC R & M No.3116 (1957)
4	J.H.B. Smith	Boundary conditions on a vortex sheet. Unpublished MOD(PE) Material, ARC 33540 (1971)
5	D.I. Pullin	A method for calculating inviscid separated flow about conical slender bodies. ARL (Australia) Aerodynamics Report 140 (1973)
6	J.E. Barsby	Separated flow past a slender delta wing at low incidence. Aero. Quart., 24, 2, 120-128 (1973)
7	I.P. Jones	Leading-edge vortex flows. Ph.D. Thesis, University of East Anglia (1974)
8	A.H. Sacks R.E. Lundberg C.W. Hanson	A theoretical investigation of the aerodynamics of slender wing-body combinations exhibiting leading-edge separation. NASA CR-719 (1967)
9	P.T. Fink W.K. Soh	Calculation of vortex sheets in unsteady flow and applications in ship hydrodynamics. University of New South Wales, Report/Nav Arch/74/1 (1974)
10	D.W. Moore	A numerical study of the roll-up of a finite vortex sheet. J. Fluid Mech., 63, 2, 225-235 (1974)

REFERENCES (concluded)

No.	Author	Title, etc.
11	C. Rehbach	Etude numérique de nappes tourbillonnaires issues d'une ligne de décollement près du bord d'attaque. La Recherche Aerospatiale, No.1973-6, pp.325-330 (1973)
12	J.A. Weber G.W. Brune F.T. Johnson P.A. Lu P.E. Rubbert	A three-dimensional solution of flows over wings with leading-edge vortex separation. AIAA 8th Fluid & Plasma Conference, AIAA Paper 75-866 June 1975
13	J.H.B. Smith	Similar solutions for slender wings with leading-edge separation. 13th Int. Congr. Th. and Appl. Mech. Moscow (1972)
14	W.P. Jones	Trends in unsteady aerodynamics. 6th Lanchester Memorial Lecture (1962) Journ. R. Ae. Soc. 67, 137-152 (1963)
15	R.K. Nangia G.J. Hancock	Delta wings with longitudinal camber at low speeds. ARC CP No.1129 (1970)
16	M.H. Snyder	Some effects of camber on swept-back wings. Society of Automotive Engineers, Paper 730298 (1973)

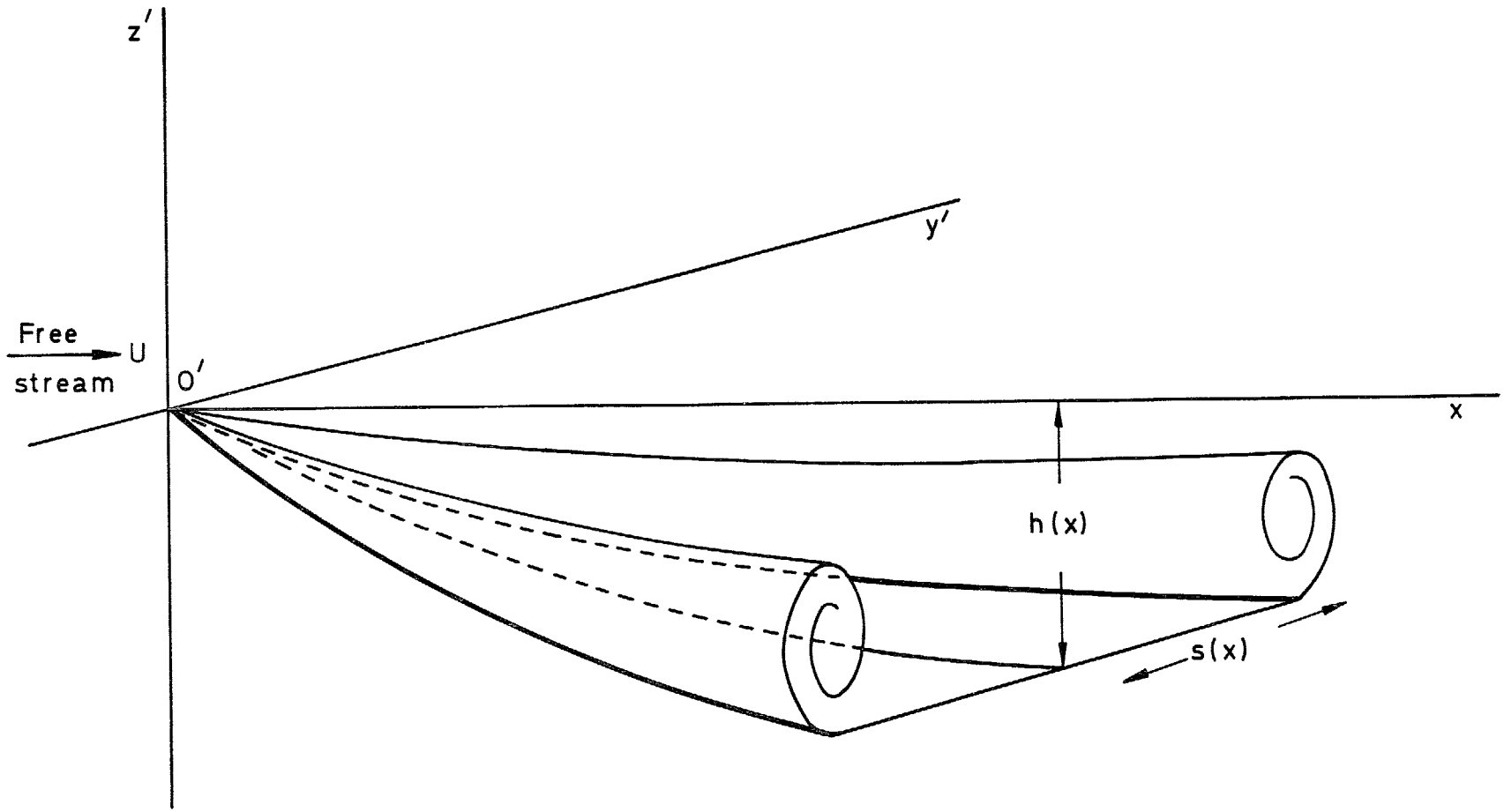

Fig.1 Typical wing, vortex sheets and axis system

Fig.2a&b

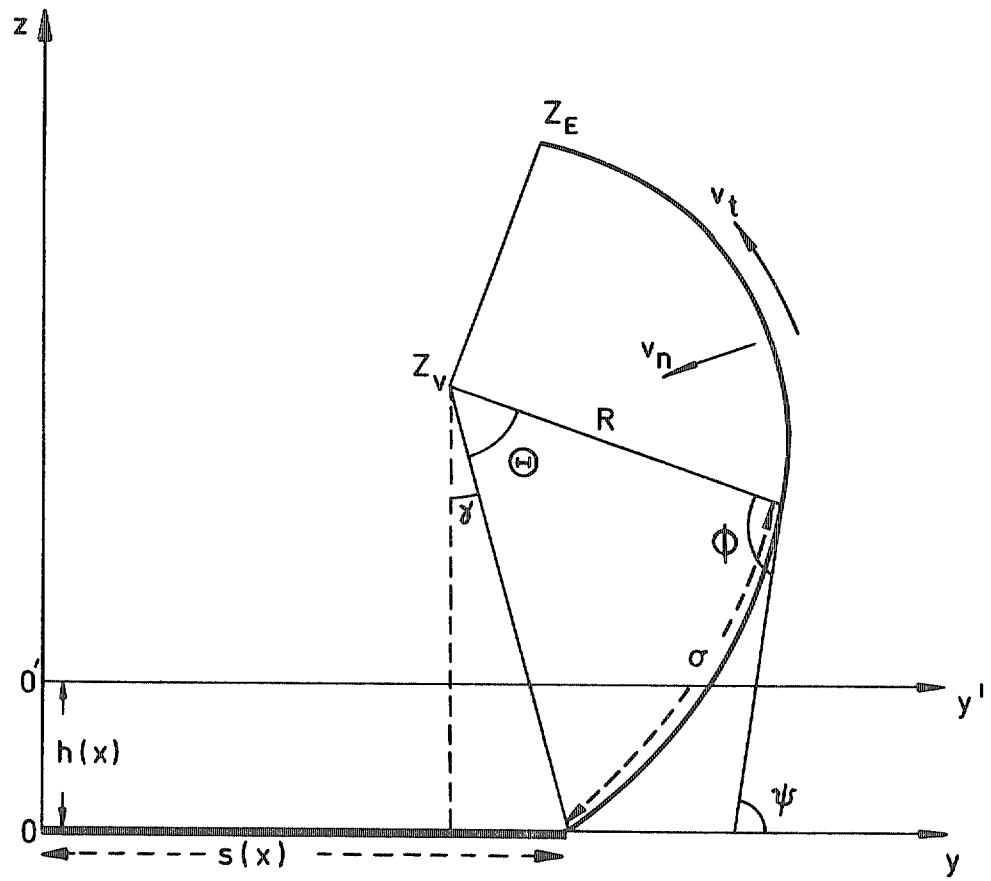

a The cross-flow plane

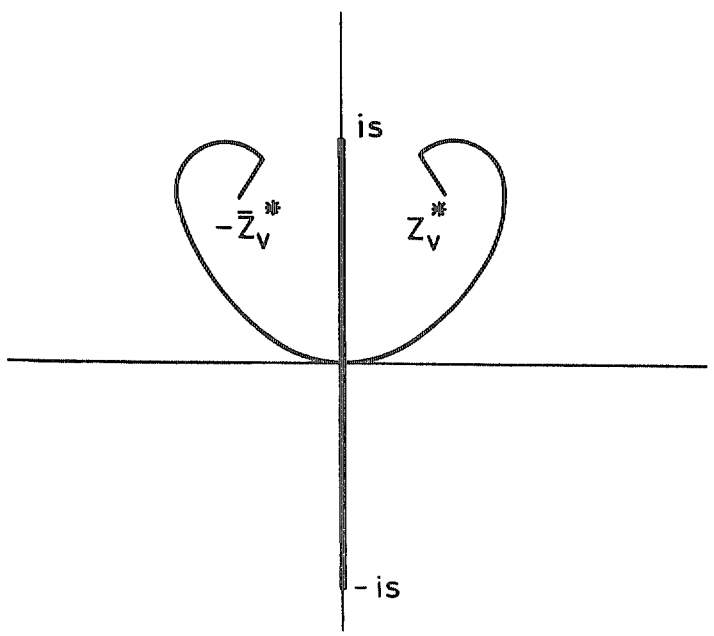

b The transformed plane

Fig.2a&b The coordinate systems

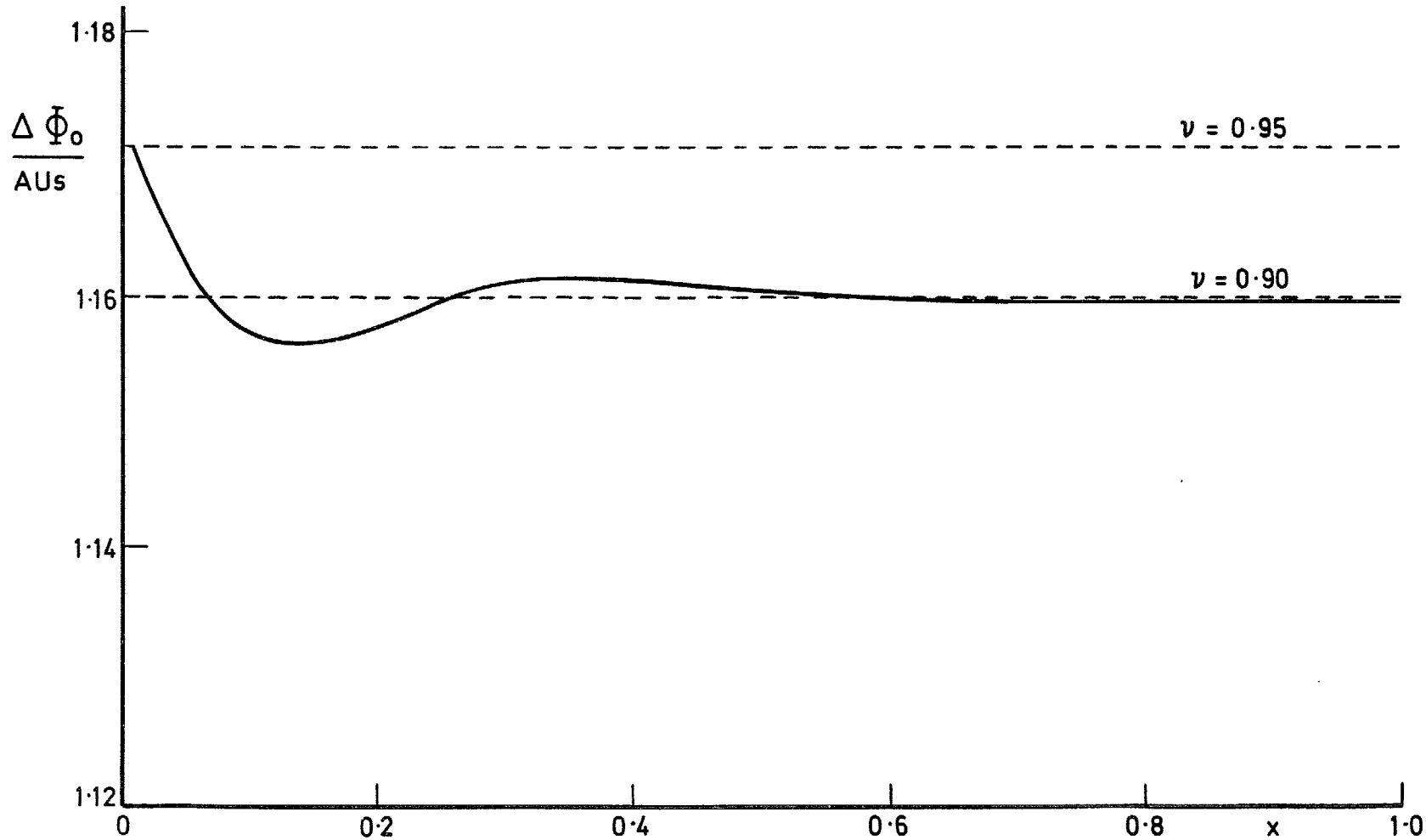

Fig.3 Adjustment of total circulation for wings of self-similar form

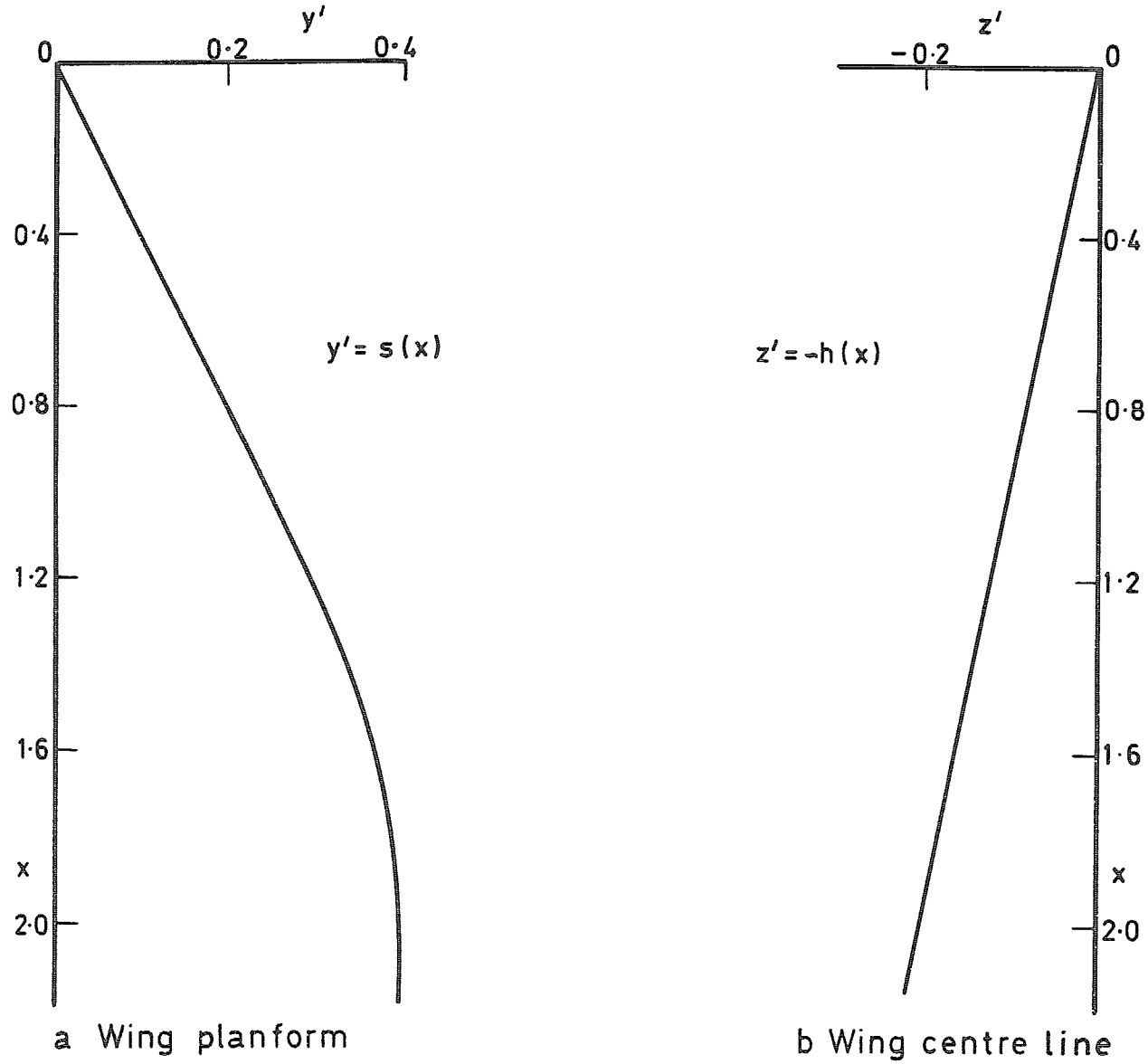

Fig.4a&b Plane wing with curved leading edge

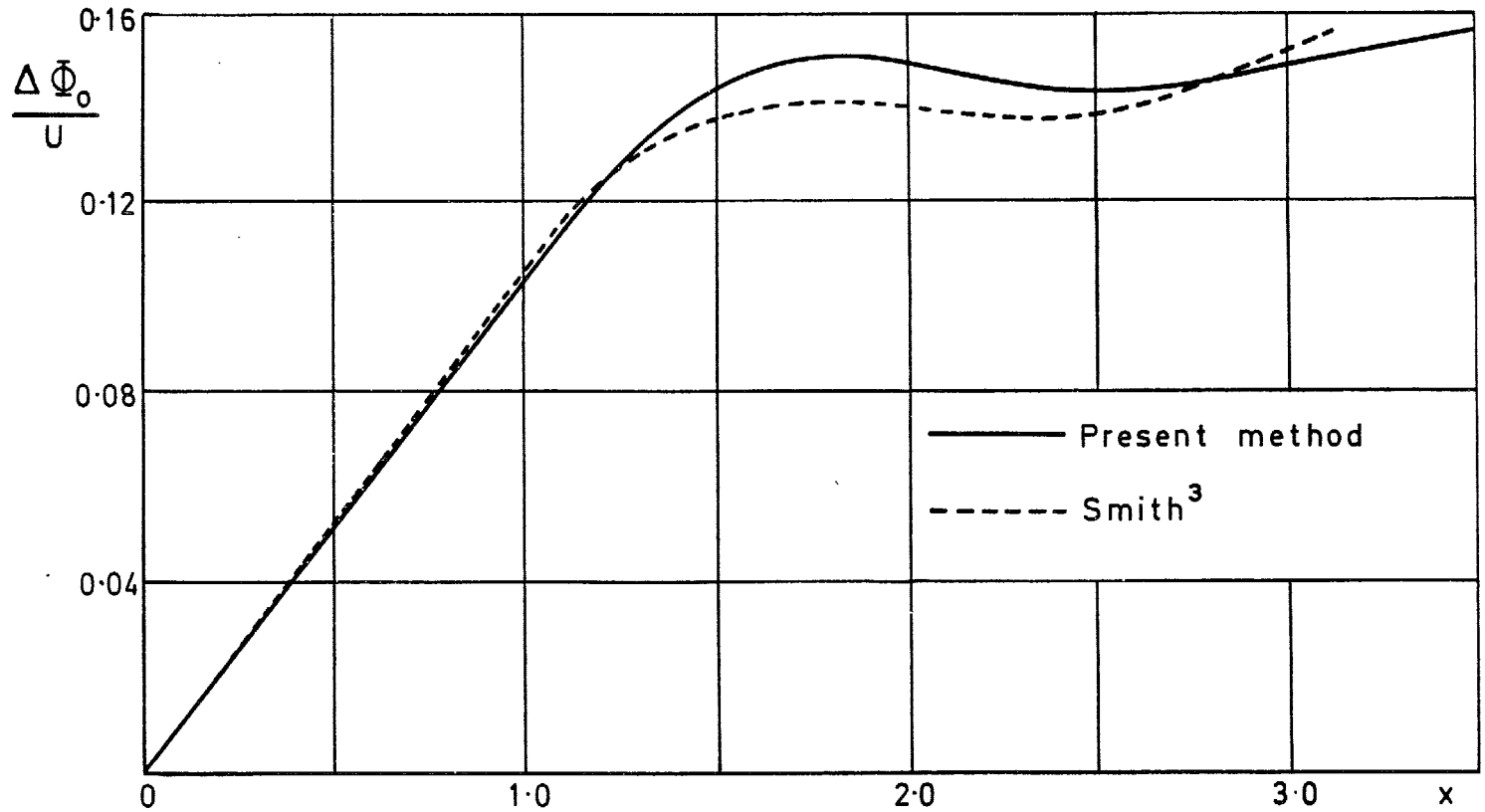

Fig 5 Total circulation. Curved leading edge wing

Fig 6

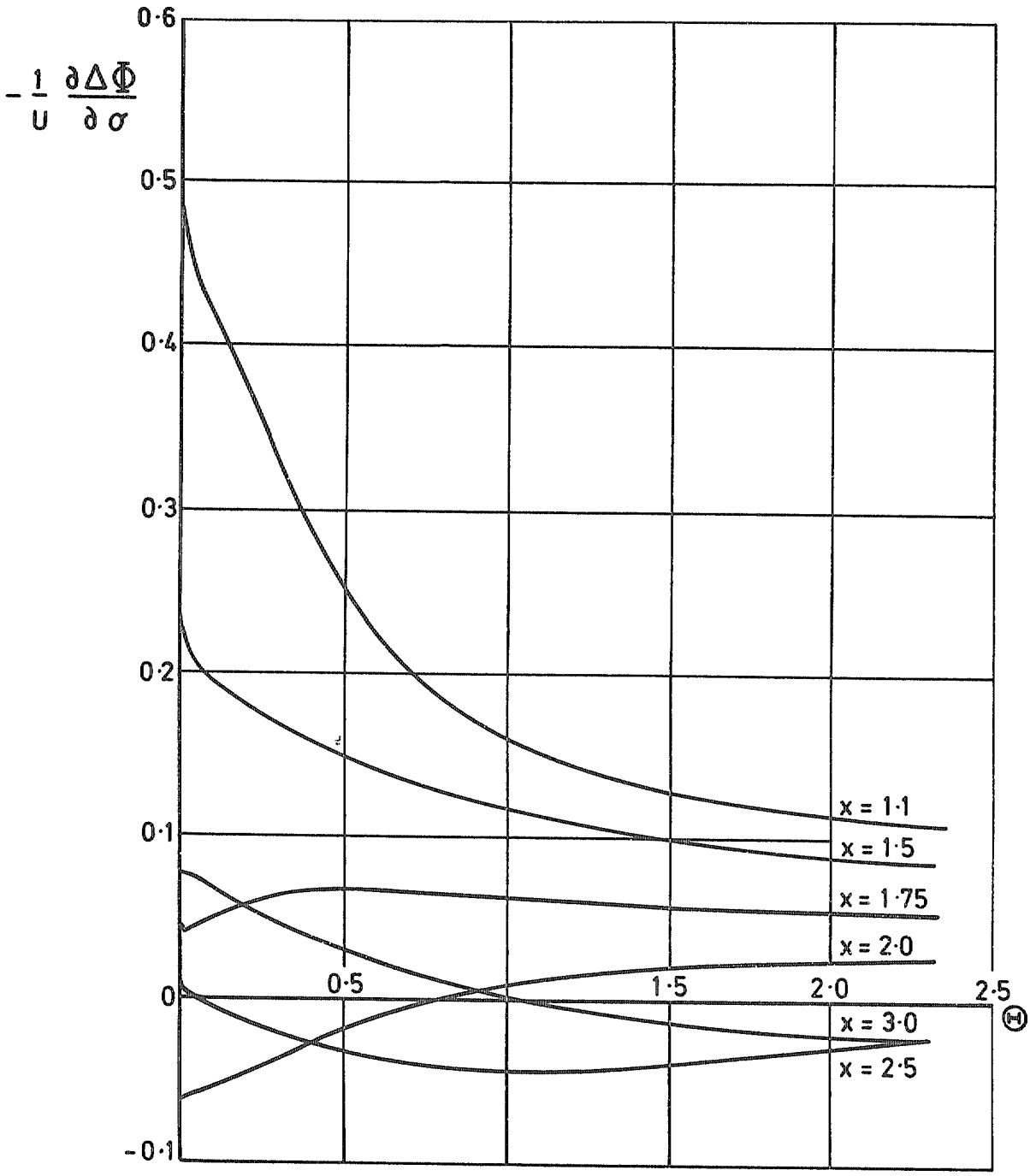

Fig.6 Vortex sheet strength. Curved leading edge wing

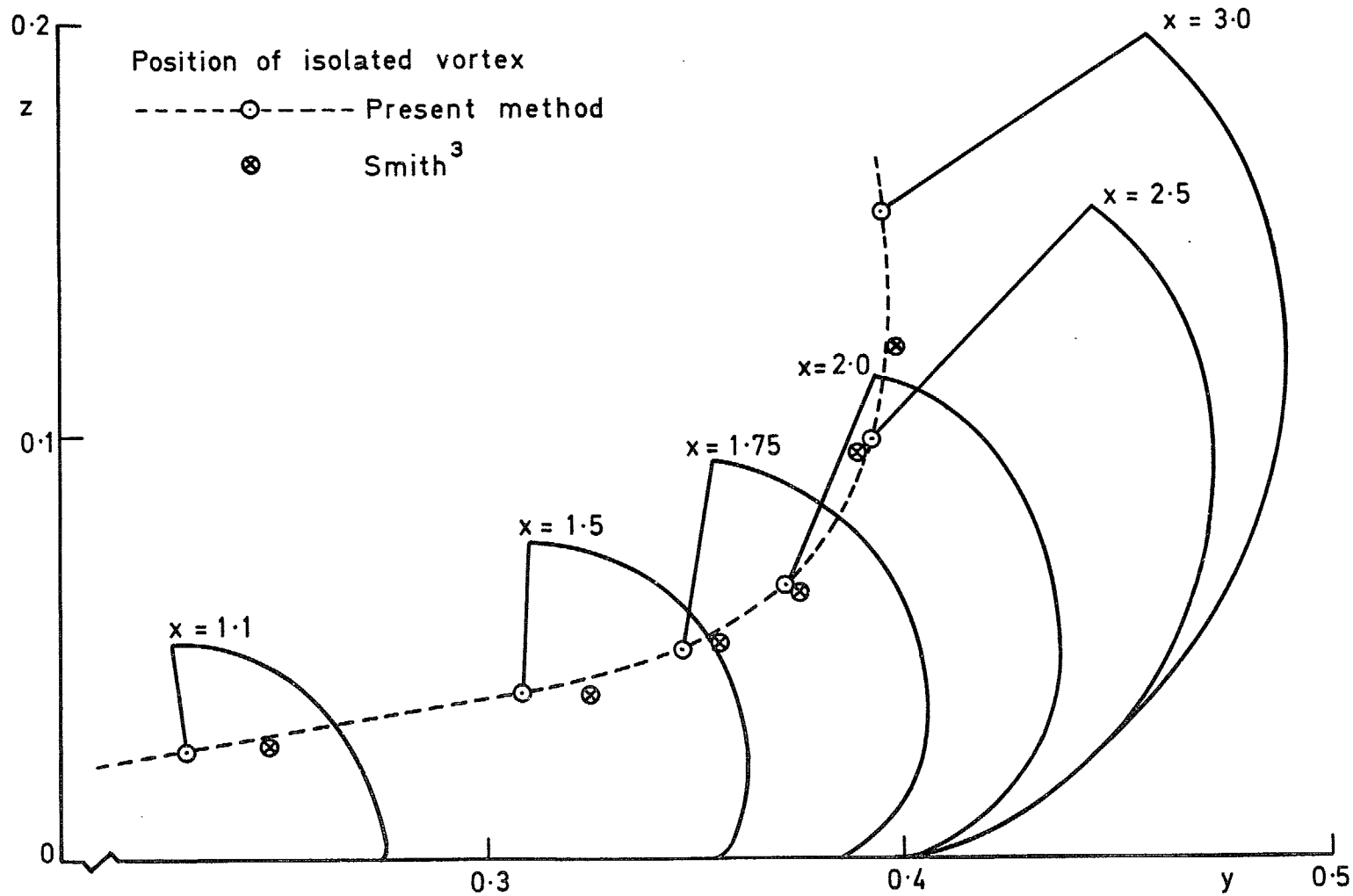

Fig.7 Vortex sheet shape. Curved leading edge wing

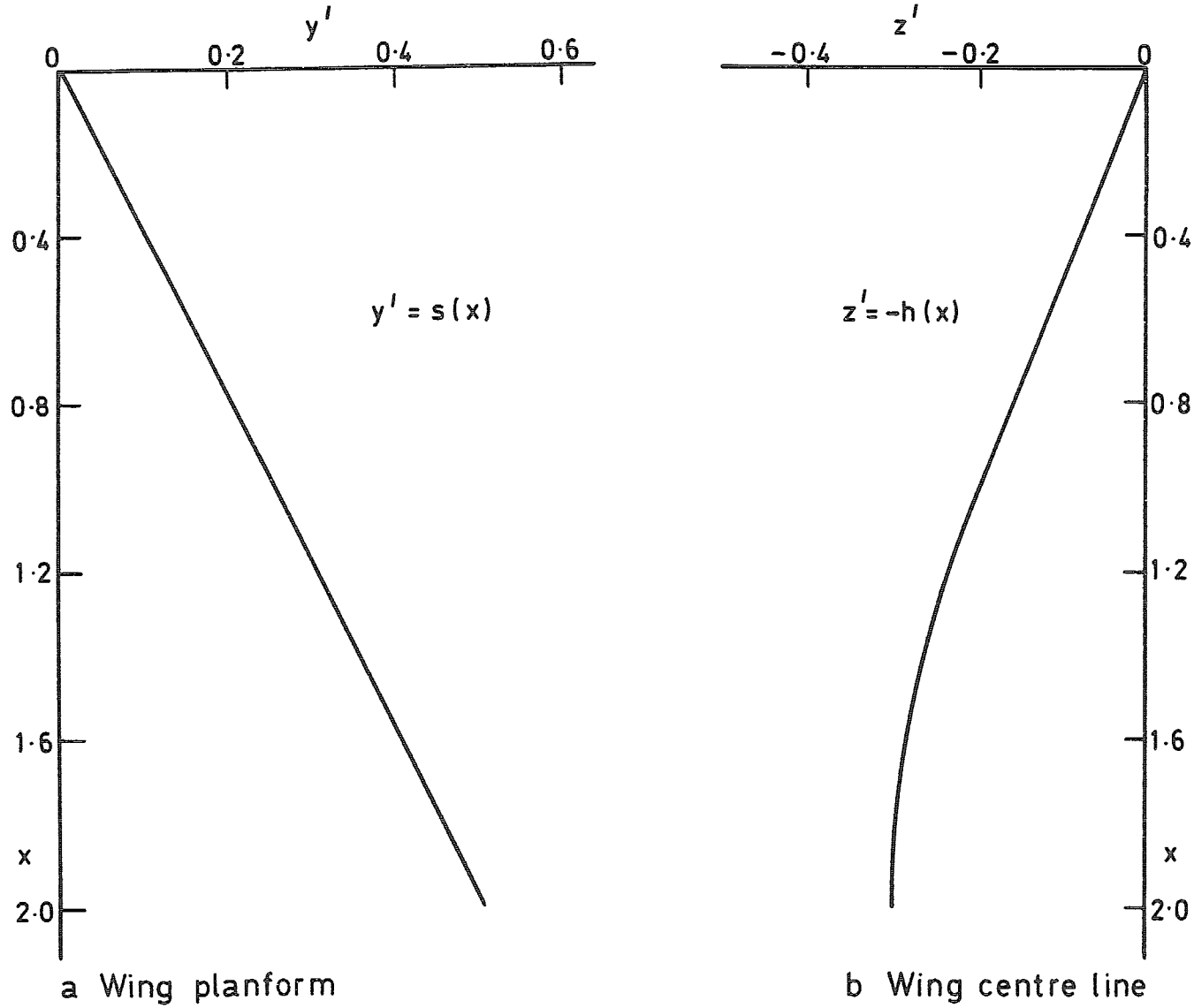

Fig.8a&b Delta wing with lengthwise camber

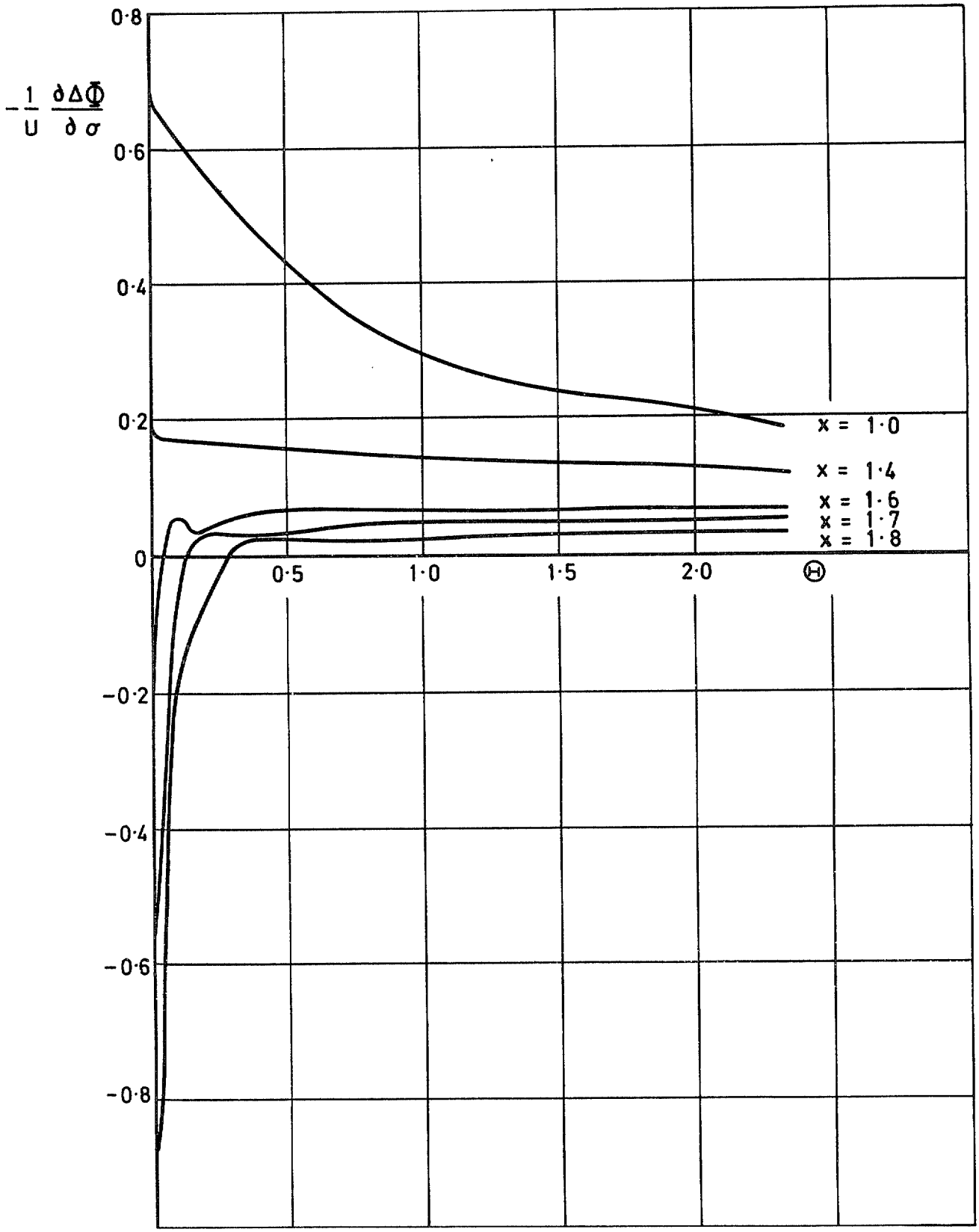

Fig.9 Vortex sheet strength. Cambered delta wing

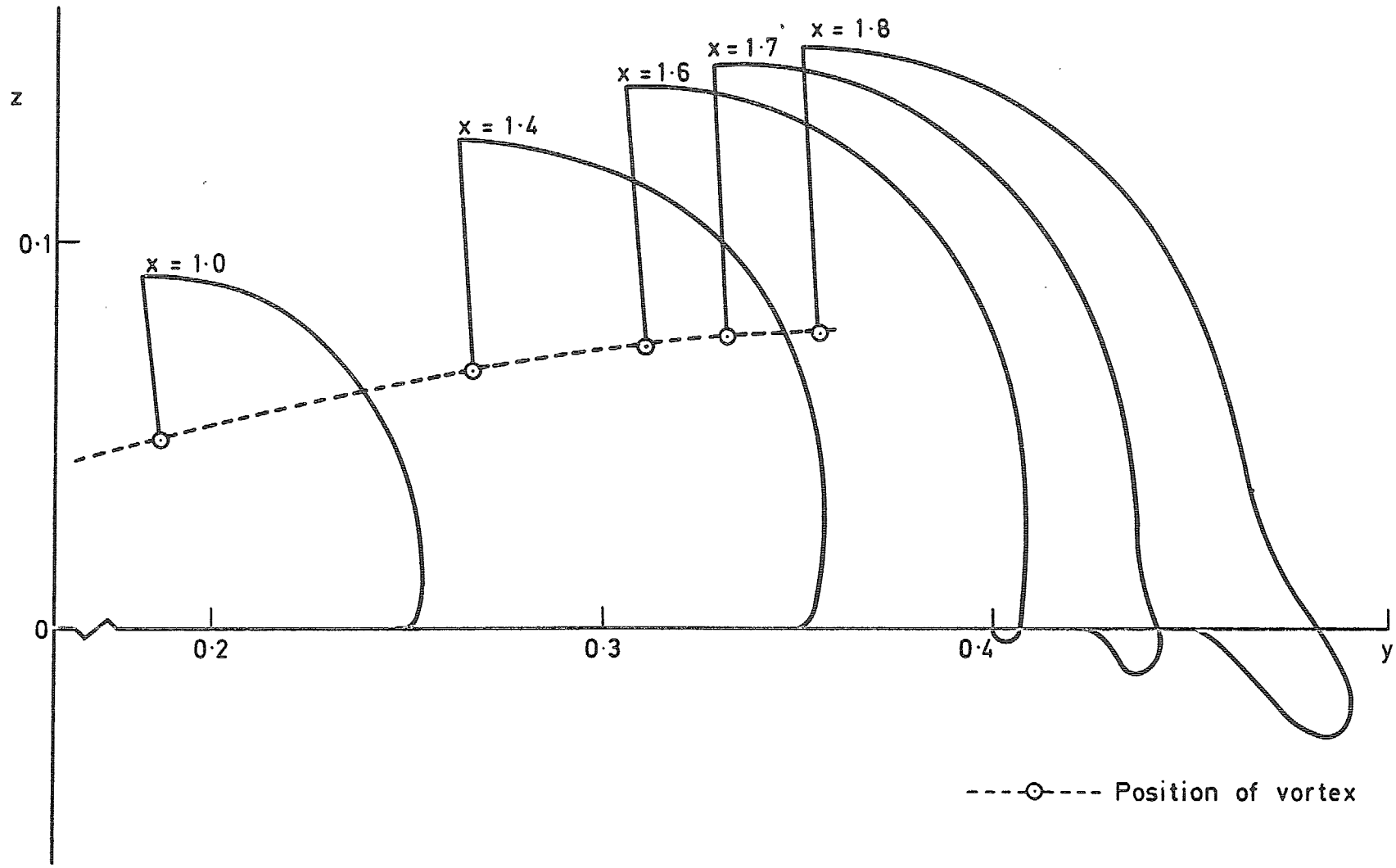

Fig.10 Vortex sheet shape. Cambered delta wing

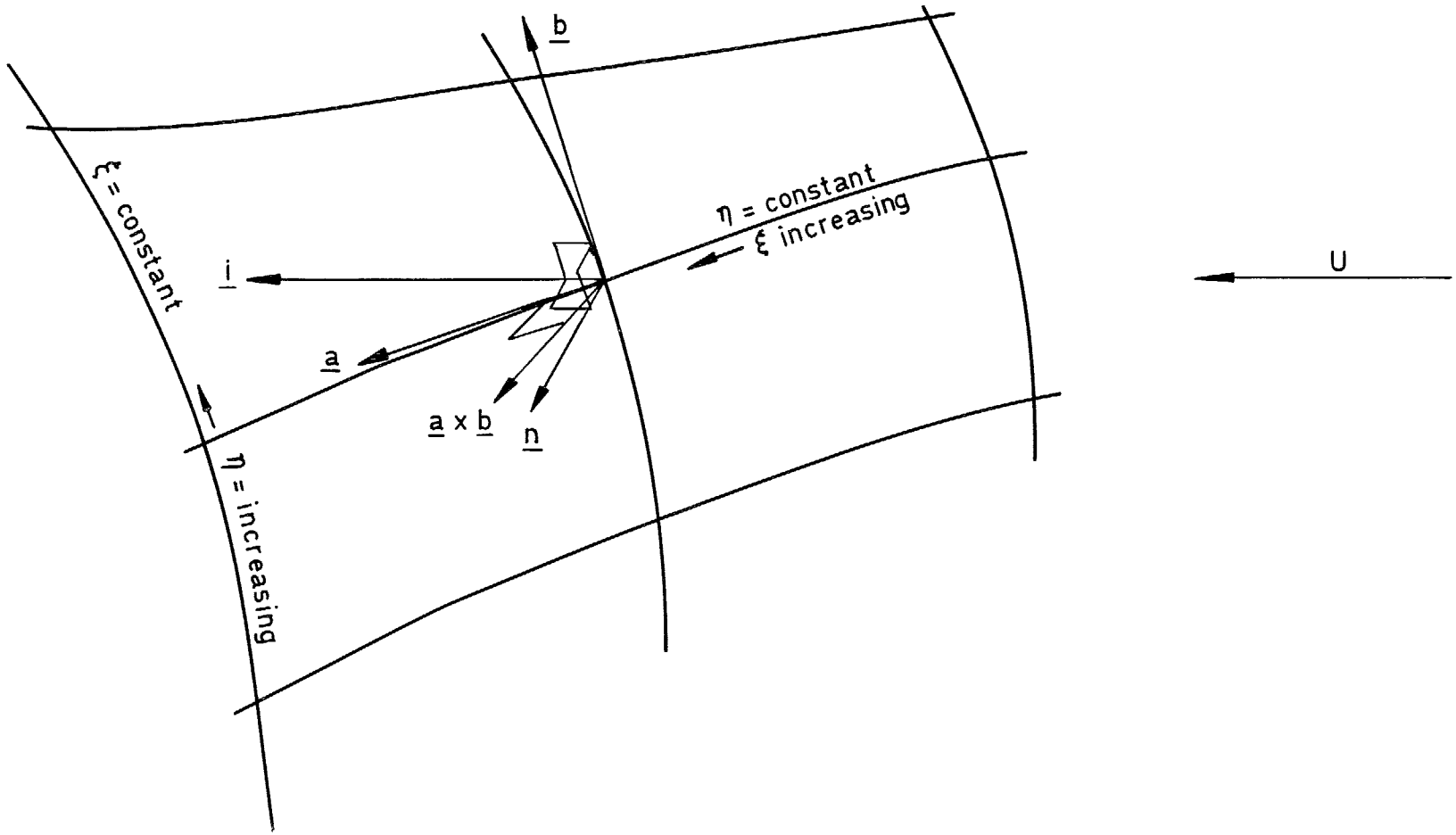

Fig.11 The vortex sheet, Σ

Fig 11

Fig.12a

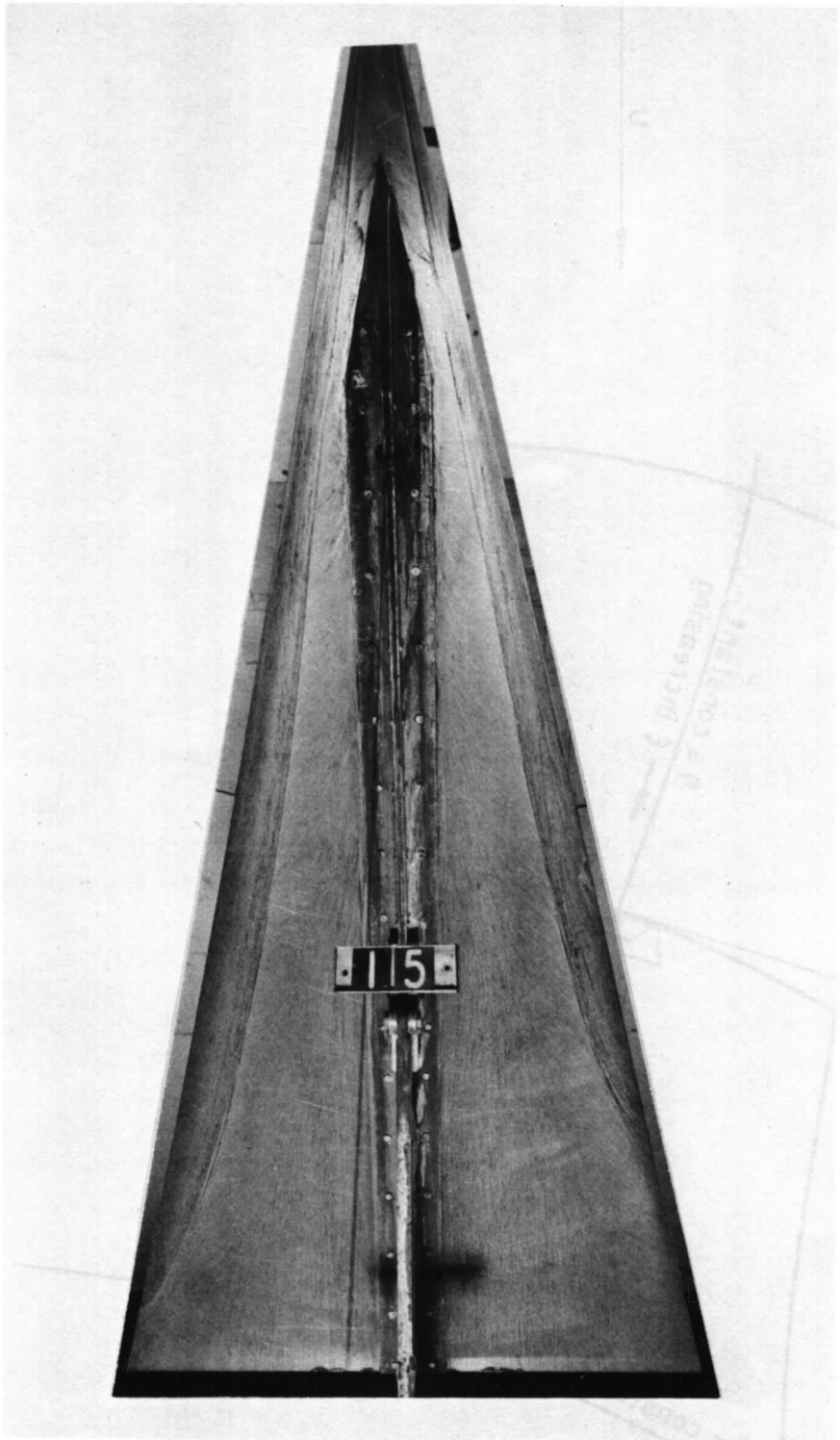

Fig.12a Concave surface oil flow — 15° apex incidence

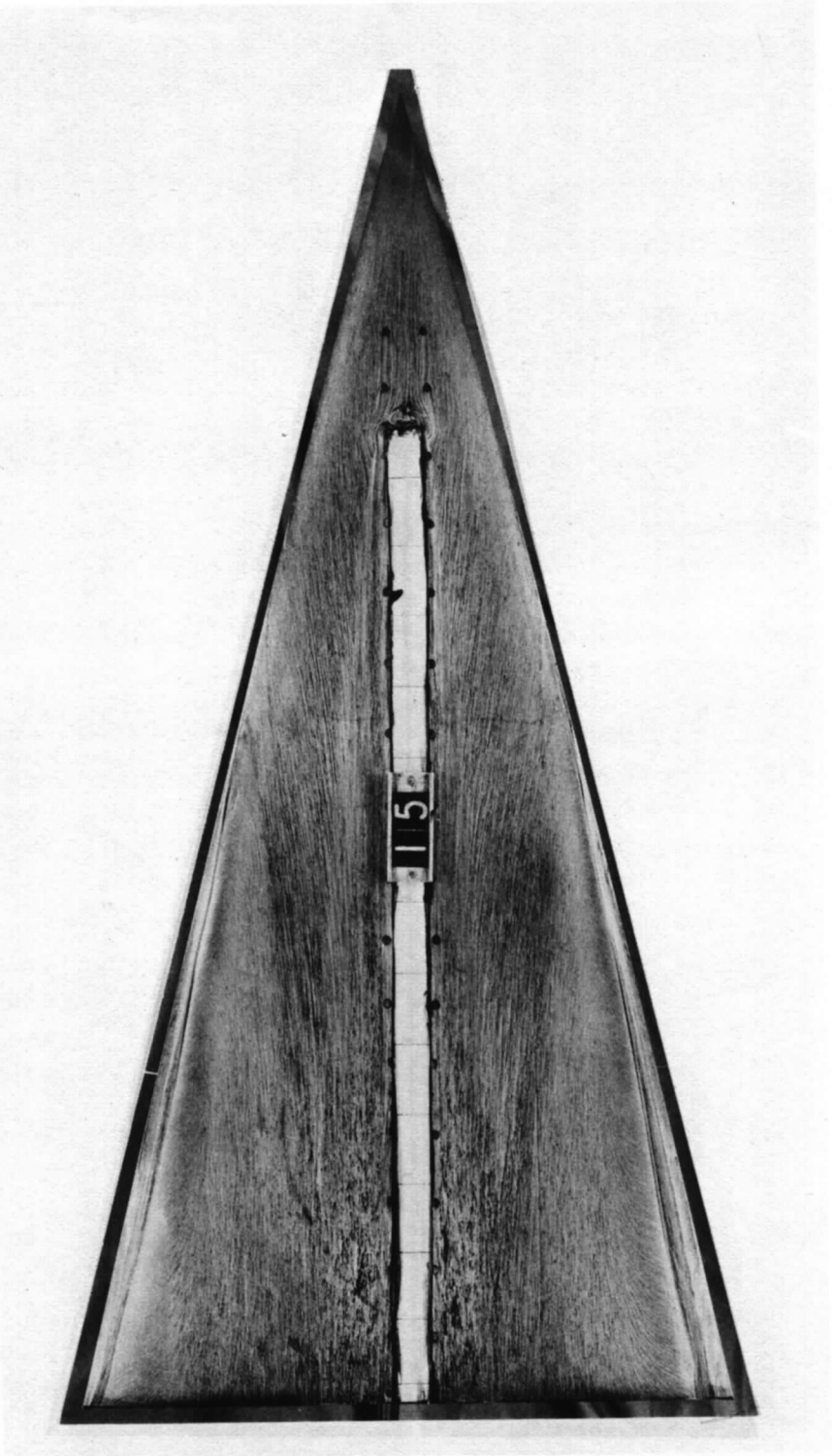

Fig.12b Convex surface oil flow — 15° apex incidence

Fig.12c

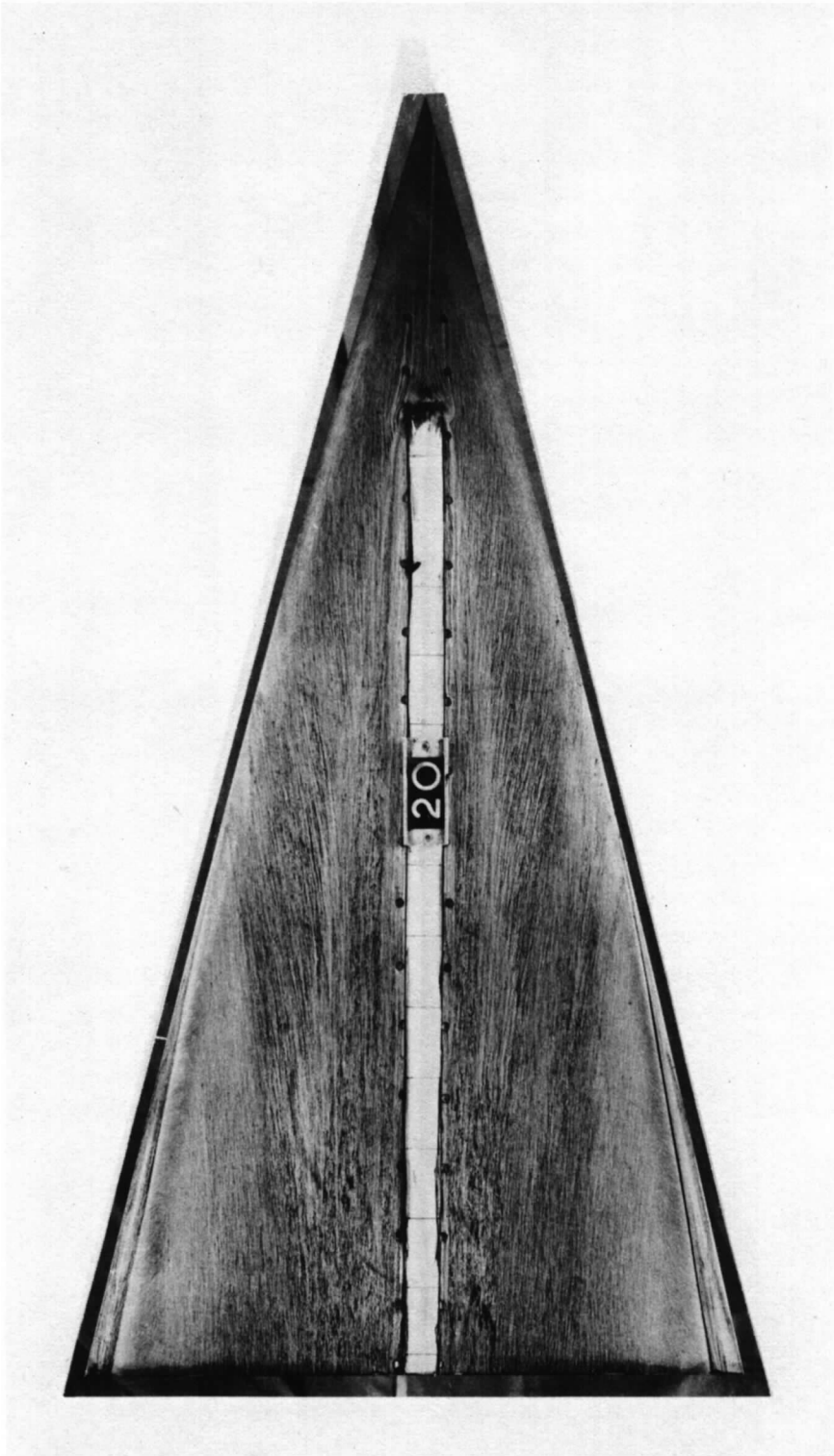

Fig.12c Convex surface oil flow – 20° apex incidence

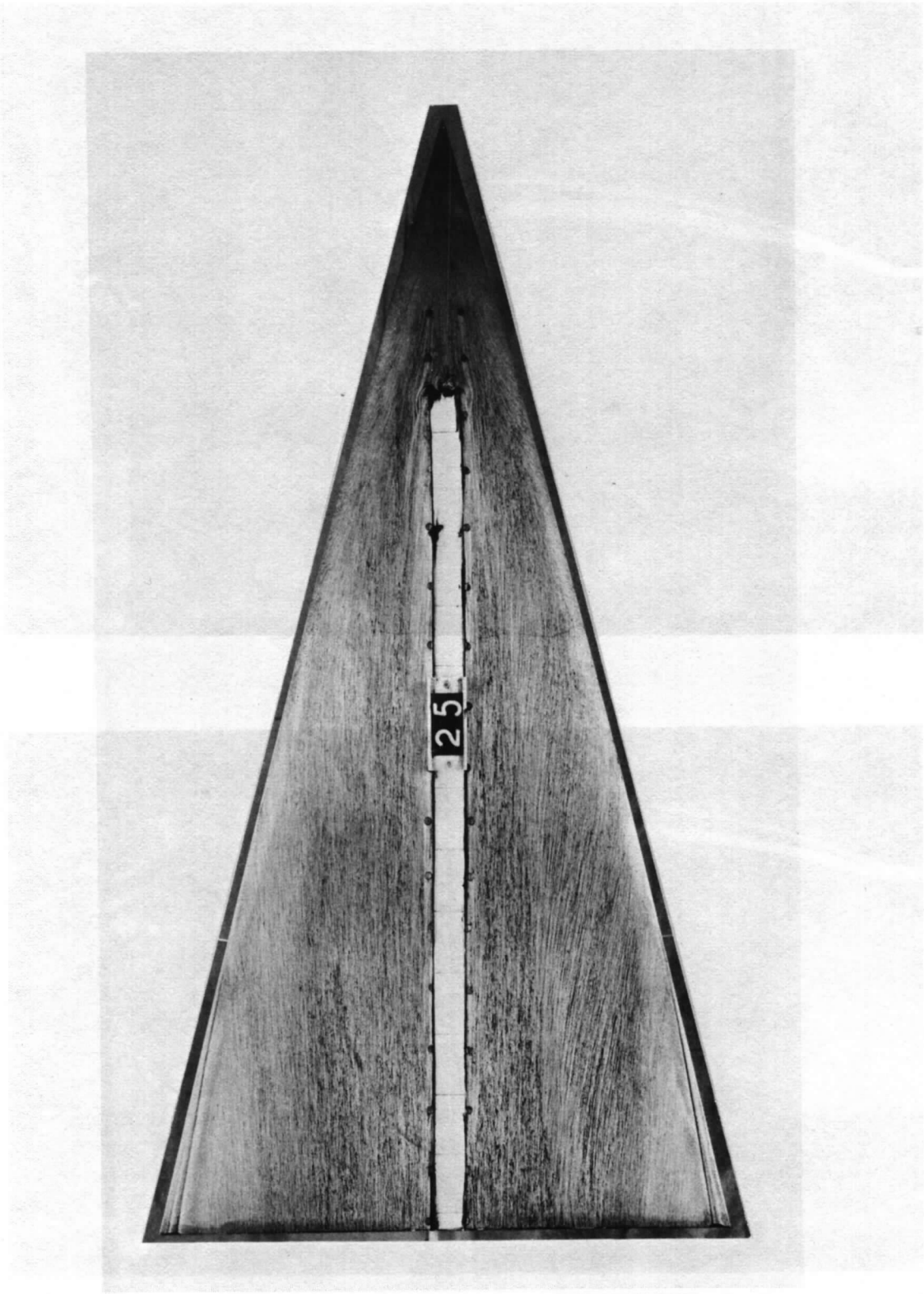

Fig.12d Convex surface oil flow – 25° apex incidence

Fig.13a&b

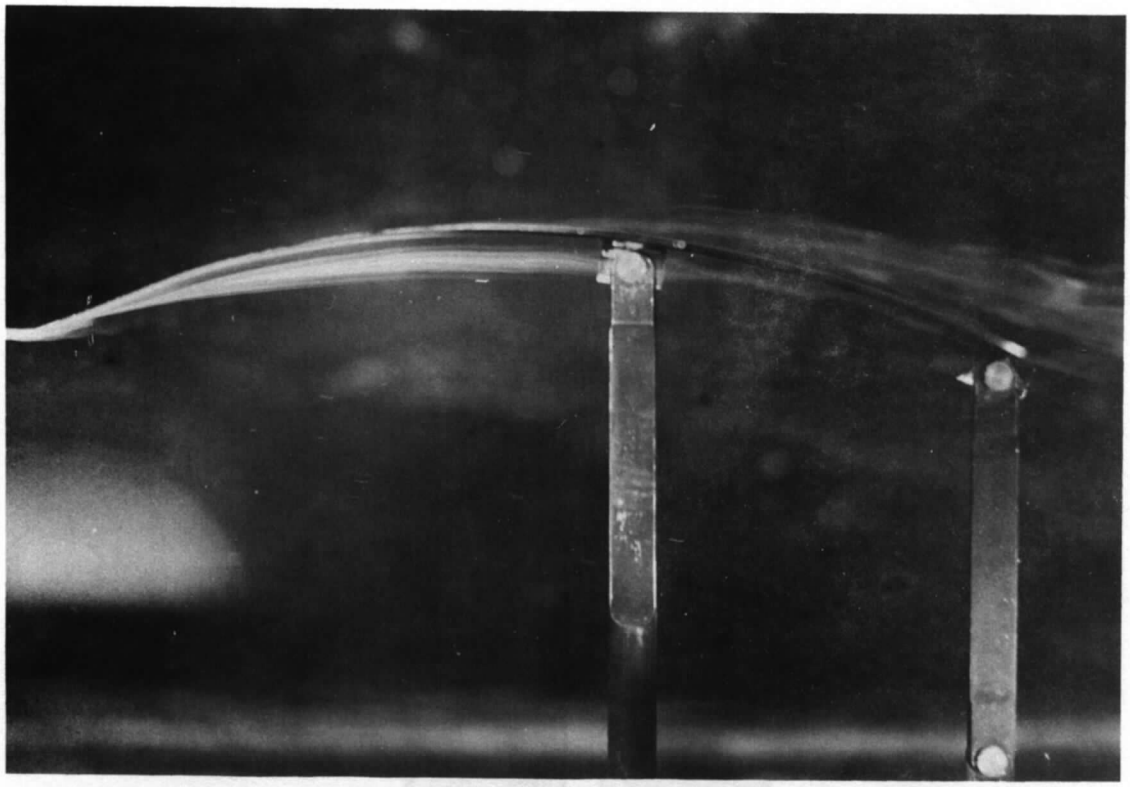

a.

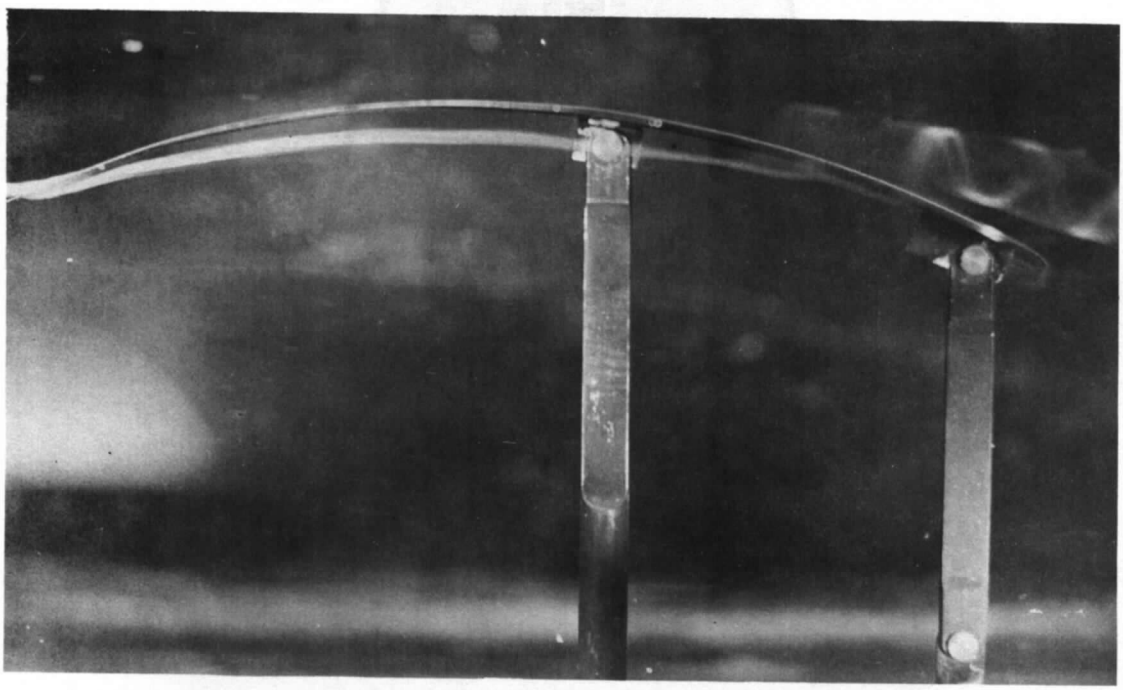

b.

Fig.13a&b Water tunnel test of cambered elta wing

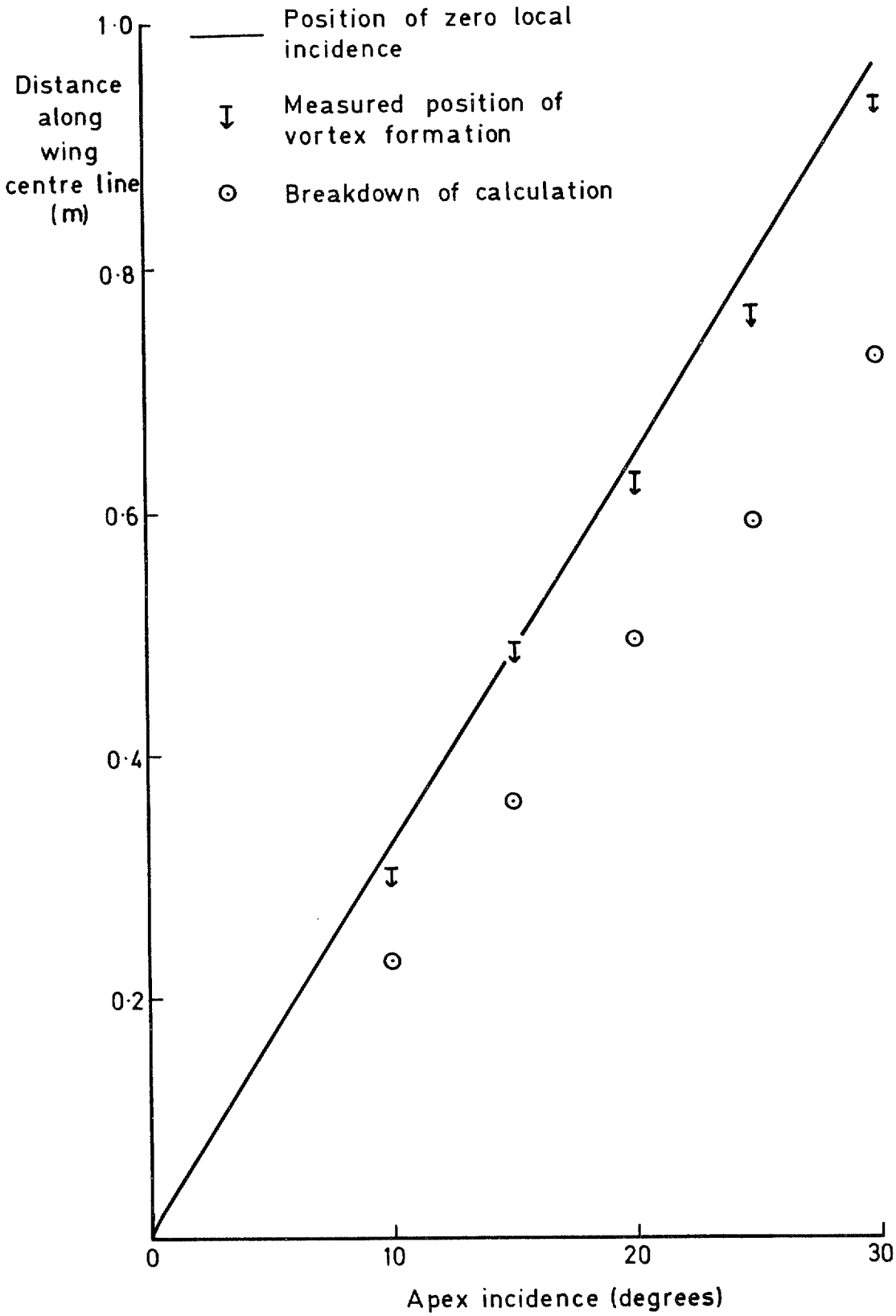

Fig.14 Formation of second vortex on wing with lengthwise camber

Printed in England for Her Majesty's Stationery Office by the Royal Aircraft Establishment, Farnborough. Dd. 587484 K4 3/78.

Published by
HER MAJESTY'S STATIONERY OFFICE

Government Bookshops
49 High Holborn, London WC1V 6HB
13a Castle Street, Edinburgh EH2 3AR
41 The Hayes, Cardiff CF1 1JW
Brazennose Street, Manchester M60 8AS
Southey House, Wine Street, Bristol BS1 2BQ
258 Broad Street, Birmingham B1 2HE
80 Chichester Street, Belfast BT1 4JY

Government Publications are also available through booksellers

R &M No.3814
ISBN 0 11 471147 X